ASTRONOMY & ASTROPHYSICS SUPPLEMENT SERIES

Astron. Astrophys. Suppl. Ser. 65, 111-144 (1986)

VLA observations of low luminosity radio galaxies. II. Sources with angular size larger than two arcminutes

H. R. de Ruiter (1), P. Parma (1), C. Fanti (1,2) and R. Fanti (1,2)

- (1) Istituto di Radioastronomia, Via Irnerio 46, 40126 Bologna, Italy
- (2) Dipartimento di Astronomia, Universita' di Bologna, Via Zamboni 33, 40126 Bologna, Italy

Received August 20, accepted November 5, 1985

Summary. — We present VLA observations of 35 radio sources selected from two samples of low luminosity B2 radio galaxies. All 35 sources are more extended than 2 arcmin and were observed at 20 cm with the C-configuration of the VLA, the angular resolution being about 13 arcsec. The present data, together with the observations presented in Parma et al. (1986, in press), cover about 80 % of the two B2 samples. The remaining 20 % consists mainly of well studied sources (e.g. 3C 31, 3C 310), so that mapping with high resolution at 20 cm of the total sample may now be considered essentially complete. We describe first the reduction procedure and discuss the quality of the radio maps. The dynamic range in the final CLEANed maps is usually around 100: 1 or better. We give in separate tables the observational parameters and intrinsic properties derived for each source. We present contour maps for all sources, but in addition also radio photographs for sources with complicated structures that are not easily recognized from the contour maps. Information on individual sources is provided, particularly in case of interesting structures.

Key words: radio galaxies.

1. Introduction.

Many B2 radio galaxies have been observed by us at high angular resolution with the VLA. These observations were carried out at 20 cm with the VLA in the B configuration (Parma et al., 1986, in press, Paper I) and in the A configuration (Fanti et al., 1986, Paper III).

Several other B2 radio galaxies have an angular size larger than 2 arcmin, which makes them less suited for observation with the A and B-configurations, since significant portions of such sources would be resolved out. We therefore selected the extended sources for observation with the C-configuration (always at 20 cm wavelength) and give the results in the present paper.

The radio sources discussed here and in paper I comprise about 80 % of all sources in the two complete B2 samples (defined in Colla et al., 1975, — the «bright» sample; and Fanti et al., 1978, the « faint » sample). The remaining 20 % consists of well studied sources, which have been discussed in great detail by various authors, and of a few misidentifications. It falls beyond the scope of the present article to redefine and rediscuss the entire collection of B2 low luminosity radio galaxies, but we intend to do so elsewhere in the near future.

Very little radio data existed for sources of the faint B2 sample, which happen to be on average more extended

Send offprint requests to: H. R. De Ruiter.

than two arcminutes. The new observations presented here remedy this lack of information completely and open the possibility to perform a statistical study of the properties of low luminosity radio galaxies on the basis of about 100 objects.

In section 2 we discuss the selection of the 35 sources that were observed with the VLA C-configuration and the data reduction procedure.

In section 3 we give the results in the form of radio contour plots (and some radio photographs) and of tables, in which the observed and intrinsic radio source parameters are summarized.

Finally, in section 4, comments are given on a number of sources.

2. Observations and data reduction.

A description of the VLA and its modes of operation can be found in Thompson et al. (1980).

We selected 35 sources from the two B2 samples, almost all having an angular size larger than two arcmin, for observation at 20 cm with the C-configuration of the VLA. Three sources (0120+33, 1339+26 and 1658+32) were already included in paper I, since they had been observed also with the VLA B-configuration. Six more sources (0034+25, 0755+37, 1102+30, 1658+30, 1422+26and 1827+32) were also observed with the B-configuration, but we present both the high and low resolution data for the first time here. In a few cases (1102+30 and 1658+30) the visibility data of observations done with different VLA configurations were combined and used with equal weight in the Fourier Transform. The resulting radio maps are similar in angular resolution to the maps made with the high resolution data only, but reproduce much better the extended, diffuse regions. Thus the advantage of such combined maps is that they show together high and low resolution features.

The VLA is now capable of observing simultaneously at two (not too different) frequencies. The B-configuration observations were done before this possibility existed and only one observing frequency (1465 MHz) was used. The C-configuration observations were done at 1435 and 1665 MHz. In the following we usually refer only to the 1435 MHz observations, unless otherwise stated.

The observations were done in May 1984. Each source was observed for a time between 10 and 40 min, at frequencies 1435 and 1665 MHz, both with a bandwidth of 50 MHz.

The resulting full width at half maximum of the synthesized beam is about 13 arcsec at 1435 MHz and proportionally smaller at 1665 MHz.

A calibration source was observed immediately before or after a program source. The flux densities were brought on the scale of Baars et al. (1977), using 3C 48 and 3C 286 as primary flux calibrators. Flux densities of other calibration sources were bootstrapped from the flux densities of 3C 48 and 3C 286. Raw data were checked for deviating amplitudes, which were edited out.

Post-calibration reduction was done at the VLA site, using the NRAO-AIPS package. The procedure followed was identical to the one described in paper I.

Since the field of view for 20 cm C-configuration observations is large, confusion by strong background sources sometimes complicated the reduction. These problems were overcome either by increasing the map size from the standard 512 by 512 to 1024 by 1024 pixels (always with a step of 4 arcsec per pixel), or by making small maps centered on the (known) positions of disturbing sources and cleaning these maps simultaneously with the central program source. The clean components thus obtained were subtracted in the UV plane and the process was then repeated on the resulting UV data until convergence was reached. (This powerful method was recently introduced into AIPS.)

The radio maps obtained in this way were usually the final ones: their r.m.s. noise was mostly within three times the thermal receiver noise. Several trials with self-calibration showed in general no significant improvement in the quality of the maps. Therefore self-calibration was applied only in a few cases (e.g. 0828 + 32).

Since we are interested mainly in the structure and strength of the radio sources at 20 cm (as in Papers I and III), we present only the 1435 MHz data; we just remark that 1665 MHz data (source parameters and radio maps) do exist.

Following paper I we list in tables Ia and Ib the observational parameters for the bright and faint samples respectively. We give the source name, the observing time per source, the FWHM of the synthesized beam and the r.m.s. noise in the final 1435 MHz map. The r.m.s. noise in the

final map is for most fields in the range 0.2-0.4 mJy/beam, which should be compared with a receiver noise of 0.1 to 0.2 mJy/beam, depending on the observing time.

Observational parameters of the VLA B-configuration data for the sources 0034+25, 0755+37, 1102+30, 1422+26, 1658+30 and 1827+32 can also be found in tables Ia and Ib.

No systematic analysis of polarization has been carried out, since the signal to noise ratio is not adequate to study the whole source sample. However, some sources do show significant polarization. These results will be presented elsewhere.

3. Results.

In the following we shall refer to the B- and C-configuration observations as high and low resolution data.

Source parameters are given in tables IIa and IIb. The organization of this table is identical to the one of table II in paper I. For the six sources mentioned in the previous section the high resolution data were used to derive parameters for cores and jets, while the low resolution data were used for the extended components. When no high resolution data exist, it is difficult to disentangle the radio core and jets from the surrounding emission. In such cases we use the term central component instead of core in table II.

In general the VLA total flux densities derived for the sources described here agree well (within 20%) with the flux densities measured by us with the WSRT. There are four exceptions, however: 0828+32, 0836+29 and 1658+32 have a VLA flux density about 30% lower than the WSRT flux. For 0915+32 the VLA flux is lower by even more than 50%. Inspection of these sources on the WSRT maps reveals very extended low surface brightness regions. Considering that the shortest baseline in the VLA observations is 63 m, as compared to 36 m at Westerbork, we obviously have lost a large part of the low surface brightness flux. We decided to give in table III the WSRT radio powers for these four sources (marked by an asterisk).

One source (1555+30) was found to be a misidentification, since the optical position of the galaxy falls between two radio sources that are almost certainly unrelated; in the earlier lower resolution (WSRT) map the source was mistaken for a classical double. There is no other bright galaxy nearby that could be the optical counterpart of the radio sources; therefore 1555+30 should be excluded from the B2 samples of low luminosity radio galaxies. This source is neither given in the tables nor in the figure.

Another source (0843+31) is also likely to be a misidentification (see note), although its data and map are presented here.

In figures 1-47 we present contour maps. If also new high resolution data were available, contour maps of both the high and low resolution data, or a combination of them, are given. The high resolution maps are distinguished by the letter « H ».

A number of sources showed complicated structures that are not well visible in the contour maps. For this reason we added radio photographs of 0755+37, 0828+32, 1005+28, 1116+28, 1243+26, 1316+29, 1358+30 and

1528+29. The radio photo of 1658+30 represents a combined map from both high and low resolution data.

In tables IIIa and IIIb the intrinsic source parameters are given (except for 1457+29 which has no known redshift) rounded to the nearest integer or half-integer value. Linear sizes, internal energy density and magnetic field strength were derived as in paper I (using a Hubble constant of 100 km/s/Mpc).

4. Comments on individual sources.

4.1 THE BRIGHT SAMPLE.

0034 + 25

This source was observed before, with the WSRT, by Ekers *et al.* (1981). It is located in the Zwicky cluster 0034.4 + 2532, which has only eight galaxies brighter than $m_{\rm pg} = 15.7$ ($M_{\rm pg} = -19.5$ at the cluster distance). Even so, 0034 + 25 is a WAT source.

0120 + 33

In the higher resolution observation of paper I the very faint and diffuse eastern component was barely visible. 0755+37

The associated galaxy is rather isolated, the nearest galaxy with comparable magnitude being more than 15 arcmin away. Both high and low resolution maps and a radio photograph are shown in figures 4, 5 and 6. The source shows a strikingly large amount of substructure in both components; it may be another example of a «bubble blowing» object, like 3C 310 (see van Breugel and Fomalont, 1984). We have reobserved 0755+37 with the VLA, for several hours, in order to reach lower surface brightness levels. A detailed discussion of this source will therefore be presented elsewhere.

0915 + 32

Much flux was lost in the outermost regions of the source (compare with the maps given in Ekers *et al.*, 1981). A detailed analysis of 0915+32 can be found in Parma *et al.* (1985).

4.2 THE FAINT SAMPLE.

0828 + 32

Note the double structure of the lobes, best visible in the western component; there are two jetlike structures both terminating in their own hot spot (see the radio photograph in Fig. 12). Much flux and structure has been lost, as there are two more lobes located North and South see Parma *et al.*, 1985). Other VLA observations can be found in Machalski and Condon (1985).

0836 + 29

The radio source is associated with the brightest galaxy in Abell 690 (see Valentijn, 1979, for WSRT data). The VLA flux density is considerably below the WSRT flux.

0838 + 32

This source is associated with the brightest galaxy in Abell 695. The extended structures to the south and west are clearly visible in the WSRT map discussed by Valentijn (1979), where the source gives the impression of being a Wide Angle Tail. The East-West elongated structure is not visible in the high resolution map of Machalski and Condon (1983), but does show up in our own highest resolution data (Paper III).

0843 + 31

This source was originally believed to be a classical double (Fanti et al., 1978), the galaxy lying midway, but closer to the northern lobe. Further WSRT observations (Parma et al., 1985) and the present ones, show a somewhat more complex situation. The southern component is unresolved and is likely to be a background object. The northern component is split in two, giving the appearence of a classical, edge brightened double, unrelated to the galaxy. A remaining possibility, although not very plausible, is that only the central component is associated to the galaxy, being therefore a head-tail type source.

0922 + 26

Another VLA map can be found in Machalski and Condon (1985).

1005 + 28

Note the ringlike structure of the southern lobe, visible in the radio photo (Fig. 18).

1116 + 28

A radio photo is given in figure 20. See also Parma et al. (1985).

1141 + 37

Although not clearly seen in our radio map, since it is only at the level of the r.m.s. noise, a giant halo does exist, which surrounds the whole source (Malumyan, 1984). The nucleus is very faint, but definitely present. A higher resolution map can be found in Machalski *et al.* (1982).

1243 + 26

The radio source is associated with the cluster Abell 1609. Two galaxies, whose positions are marked in figure 24 and are given in table II, lie within the radio contours (see also Valentijn, 1979, for a 610 MHz WSRT map).

1300 + 32

This source is associated with Abell 1667 (see Valentijn, 1979, for a study of this cluster with the WSRT). Several galaxies lie within the radio contours of this source. In figure 26 we marked the galaxy we believe to be the correct identification on the basis of our new highest resolution observations (Paper III). The identification suggested here is not the one given in Fanti et al. (1978), but corresponds to galaxy a in Valentijn (1979). The source's radio structure is therefore of the WAT-type. Note that in table II and III the redshift of the original identification is given. We assume that the right identification also belongs to the cluster and has the same redshift.

1316 + 29

Studied in detail by Condon and Mitchell (1984), in the context of the precessing beam model. A lot of fine structure is seen in the lobes (see the radio photo in Fig. 1).

1339 + 26

The radio source is associated with a pair of giant galaxies in Abell 1775. The faint western extension is a small WAT (see Paper I).

1357 + 28

The NE component is unrelated to the B2 source.

1358 + 30

Certainly one of the sources in the B2 samples with a most peculiar morphology. Note the optical position of the

Astronomy and Astrophysics no 1-86 July. — 8

galaxy. There are no sharp (point or jetlike) features; in fact our more recent observations with the VLA A configuration completely resolve out the whole source. The shape of this source reminds one of a galactic source, but of course this is very unlikely at this galactic latitude. Nevertheless, we consider the identification of the source with the galaxy as uncertain.

1447 + 27

Another source at $RA = 14^{h}47^{m}22^{s}7$, $DEC = 27^{o}58'45''.1$, S = 69 mJy is unrelated to the galaxy. No map is given.

The source is resolved in the north-south direction and could be a small double. Another source of 66 mJy at $RA = 15^{\rm h}12^{\rm m}03^{\rm s}8$, $DEC = 30^{\rm o}23'11''$ is probably unrelated to the galaxy. No map is given.

1528 + 29

Note the knotty jet, well visible in the radio photo in figure 37.

1658 + 30

The radio galaxy belongs to a pair.

1658 + 32A

The source lies in Abell 2241. See Bijleveld and Valentijn (1982) for a WSRT map. Higher resolution data were given in paper I.

1827 + 32

See also Parma et al. (1985), for WSRT data.

Acknowledgements.

H. de R. and P. P. were visitors at the VLA, where all reductions were done, and wish to acknowledge the hospitality of the VLA staff. P. P. acknowledges the support of a NATO-fellowship.

The National Radio Astronomy Observatory is operated by Associated Universities, Inc., under contract with the National Science Foundation.

References

BAARS, J. W. M., GENZEL, R., PAULINY-TOTH, I. I. K., WITZEL, A.: 1977, Astron. Astrophys. Suppl. Ser. 61, 99.

BIJLEVELD, W., VALENTIJN, E. A.: 1982, Astron. Astrophys. 111, 50.

VAN BREUGEL, W., FOMALONT, E. B.: 1984, Astrophys. J. Lett. 282, L55.

COLLA, G., FANTI, C., FANTI, R., GIOIA, I., LARI, C., LEQUEUX, J., LUCAS, R., ULRICH, M.-H.: 1975, Astron. Astrophys. Suppl. Ser.

CONDON, J. J., MITCHELL, K. J.: 1984, Astrophys. J. 276, 472. EKERS, R. D., FANTI, R., LARI, C., PARMA, P.: 1981, Astron. Astrophys, 101, 194.

FANTI, R., GIOIA, I., LARI, C., ULRICH, M.-H.: 1978, Astron. Astrophys. Suppl. Ser. 34, 341.

Machalski, J., Maslowski, J., Condon, J. J., Condon, M. A.: 1982, Astron. J. 87, 1150.

Machalski, J., Condon, J. J.: 1983, Astron. J. 88, 143.

Machalsky, J., Condon, J. J.: 1985, Astron. J. 90, 5. Malumyan, V. G.: 1984, Sov. Astron. Lett. 10, 35.

PARMA, P., EKERS, R. D., FANTI, R.: 1985, Astron. Astrophys. Suppl. Ser. 59, 511.

THOMPSON, A. R., CLARK, B. G., WADE, C. M., NAPIER, P. J.: 1980, Astrophys. J. Suppl. Ser. 44, 151.

VALENTIJN, E. A.: 1979, Astron. Astrophys. Suppl. Ser. 38, 319.

 ${\it Table \ Ia.} - {\it Observational \ parameters.}$

Name	Obs.time	beam	PA	noise
	min	arcsec	degrees	mJy/beam
0034+25	28	16.3 x 13.5	88	0.21
	34	3.6 x 3.3	15	0.15
0120+33 NGC 507	29	17.2 x 13.2	-74	0.24
0755+37	14	12.0 x 11.8	44	0.65
NGC2484	30	3.8 x 3.4	-8	0.60
0915+32	25	13.5 x 11.4	12	0.15
1102+30	3 4	12.7 x 11.4	24	0.22
	37	3.6 x 3.3	-33	0.28
1422+26	15	13.5 x 12.2	-14	0.38
	31	3.8 x 3.5	0	0.14

 ${\it Table Ib.} - {\it Observational parameters}.$

Name	Obs.time min	beam arcsec	PA degrees	noise mJy/beam
0828+32	30	17.1 x 14.6	-49	0.10
0836+29	30	13.3 x 11.8	18	0.39
0838+32	41	13.2 x 11.4	10	0.22
0843+31	12	15.5 x 14.4	54	0.28
0922+36	18	11.9 x 11.5	-41	0.29
1005+28	32	13.2 x 11.5	10	0.19
1116+28	34	13.0 x 11.6	-15	0.18
1141+37	11	13.2 x 11.8	-27	0.49
1243+26	19	13.1 x 12.0	-17	0.24
1300+32	29	12.7 x 11.4	-23	0.26
1316+29 <i>F</i>	20	12.9 x 11.9	30	0.29
1339+26	16	13.1 x 12.1	29	0.29
1357+28	13	13.6 x 12.1	-8	0.20
1358+30	19	12.8 x 11.7	30	0.23
1441+26	. 16	13.2 x 12.0	-23	0.24
1447+27	10	14.0 x 12.6	0	0.35
1455+28	10	14.0 x 12.4	2	0.25
1457+29	11	13.6 x 12.3	-21	0.13
1512+30	16	13.0 x 11.8	-28	0.16
1521+28	10	13.7 x 12.2	-13	0.34
1528+29	16	12.9 x 11.9	-29	0.13
1615+32 3C332	15	12.9 x 11.7	-26	0.63
1643+27	16	13.0 x 11.9	-24	0.14
1657+32	30	12.4 x 11.2	-28	0.27
1658+30#	16 24	12.8 x 11.8 3.8 x 3.5	-33 -8	0.45 0.32
1658+32	15	12.4 x 12.0	-38	0.43
1726+31 3C357	19	12.2 x 12.1	-44	0.55
1827+32	21 31	12.8 x 11.5 3.8 x 3.7	-24 -30	0.21 0.20

 ${\bf TABLE~IIa.} \ -- \ Observational~data.$

NAME	T	I R.A.			DEC.		z n		S(1.4)	Size		LAS
	i							pg		FWHM	P.A.	
	h	m	sec	•	•	•		-	mЈу	arcsec	deg.	arcsec
0034+25 Inn jet	00	34	26.8	25	25	26	0.0321	14.8	122 27	16 x 1.7	(90)	183
E tail MS tail								i	55 40			80 x 44 130 x 25
0120+33 NGC 507	01	20	50.7	32	59	45	0.0164	13.0	70			130
E lobe W lobe								Ì	27 40			60 x 60 60 x 60
 0755+37 MGC2484	07	55	09.2	37	55	22	0.0413	14.9	1686			138
core E lobe W lobe	07	55	09.1	37	55	21	/ [~]		212 667 675 132	1.4 x 0.9		80 x 48 66 x 60
E jet 0915+32 central N jet S lobes			56.8 58		04 04	19 21	0.0620	15.5	210 18 50 148	,11 x 10	(120)	334 53 x 43 110 x <15 170 x 35
1102+30 core E lobe W lobe			39.7 39.7		25 25		0.0720	15.7	335 9 163 139	(1		170 70 x 60 70 x 60
E jet 1422+26	14	 22	26.5	 26	51	02	0.0370	15.61	>12 679	>14 x 2	(67)	140
core E lobe	14	22	26.5	26	51	02		į	10 338			60 x 60
W lobe								- 1	341			65 x 65

Table IIb. — Observational data.

HAME	R.A.	DEC.	z m 1	S(1.4) Size	LAS
	h m sec	• • •	V 	FWHM P.A. mJy arcsec deg.	arcsec
W hot spot	08 28 20.6 08 28 31.3 08 28 10.5		0.0507 15.1	1162 429 381 65 19.2 x 11.9 (146) 287 18.1 x 16.7 (118)	320 110 x 90 140 x 80
N lobe S lobe N jet	08 36 13.4 08 36 13.5	29 01 16	0.0790 14.7 	591 146 7.3 x 1.3 (20) 185 211 49	325 80 x 60 100 x 20 44 x 7
0838+32 M diffuse N compact S lobe		32 35 39	0.0680 14.8	591 66 485 11.7 x 5.5 (0) 41	128 85 x 20 70 x 30
0843+31 N lobe S lobe S comp.	08 43 38.7 08 43 33.6		0.0665 16.5 	49 24 25 54 unresolved	40 x 30 60 x 20
0922+36 central N lobe S lobe S compact	09 22 34.3 09 22 34.2 09 22 34.3	36 40 04	0.1125 15.6 	639 9 10.4 x(11.5 (175) 231 244 155 12.5 x 7.8 (25)	85 x 40 65 x 40
central N lobe S lobe	10 05 06.4 10 05 06.5	28 16 24	0.1476 16.4	77 15 26.0 x 5.2 (150) 35 27	230 55 x 50 65 x 35
1116+28 central E tail W tail		28 10 32 28 10 32	0.0667 14.3	448 132 10.1 x 3.6 (100) 143 173	260 95 x 75 130 x 60
1141+37 ME compact	11 41 50.0 11 41 57.2 11 41 56.6 11 41 41.8	37 25 06 37 26 56	0.115 16.5 	1406 627 5.2 x 4.7 (47) 150 19.1 x 12.8 (84) 522 7.0 x 2.8 (35) 107	
1243+26 central N lobe S lobe	12 43 54.6 52.7 12 43 55.5	42 32 26 44 27		382 148 57 · 177	280 90 x <10 100 x 40 105 x 75
1300+32	13 00 52.9 13 00 56.6 13 00 51.9 13 00 53.3	32 06 25 32 06 32	(0.164) 16.9 	304 95 14.0 x 8.7 (34) 14 14.8 x 8.0 (119) 195	

TABLE IIb (continued).

NAME		R.A.			DEC. z			m !	S(1.4)	Size FWHM	LAS	
	h		sec	•	•			١	mЈу	FWHM arcsec	P.A. deg.	arcsec
1316+29 central E lobe+jet W lobe+jet			43.0 43.2	29 29	54 54		0.0728	15.01		22.6 x 10.2	(30)	175 90 x 80 90 x 65
1339+26 head tail	13	39	30.7	26	37	20	0.0757	14.21	340 231 109			198 70 x 50 140 x 20
			45.2 45.2		44	28 32	0.0629	14.6	252 • 70 95 87			160 54 x 40 60 x 60
1358+30				30	36	21	0.1104	15.81	330			177 x 133
1441+26 E lobe W lobe			53	26	13	51	0.0621	14.3	227 137 90			210 80 x 50 95 x 60
1447+27			17.8 17.8	27 27	59 59		0.0306	14.2		3.6 x 1.4		
1455+28 N lobe S lobe N hot spot S hot spot	14	55			45		0.1411	16.6	773 240 188 173 172	10.4 x 6.0 15.3 x 3.2	(29)	202 100 x 65 100 x 60
1457+29 N lobe S lobe	14	57	34.4	29	15	23		17.2	309 148 162			75 x 55 40 x 30 30 x 26
1512+30			59.4 59.5		19 19	54 53	0.0931	15.4		23.6 x 5.2	(0)	
1521+28 central W lobe S lobe			21.4 21.5		48 48	07 06	0.0825	15.4		unresolved		220 60 x 60 130 x 50
1528+29 central E lobe W lobe			05.9 05.9			43 43	0.0843	15.1		unresolved		225 105 x 60 95 x 80
1615+32 3C332 N lobe S lobe Bridge	16	15	46.8	32	29	49	0.1520	16.7	2290 750 470 1090			93 x 50 35 x 15 20 x 15 60 x 50
1643+27 central N lobe S lobe			26.6 26.7		25 25	30 34	0.1017	15.8		unresolved		145 58 x 58 70 x 41
1657+32	16	57	08.6			04	0.0631		105			70 x 50
1658+30A core E lobe W lobe W jet			48.9 48.9	30	12 12		0.0351			2.3 x 1	(60)	144 70 x 65 75 x 55 48 x 8
1658+32	16	58	18.7	32	39	37	0.102	16.1	136			87 x 35
1726+31 3C357 E lobe W lobe			27.4				0.1670		1300			115 55 x 50 55 x 50
1827+32 core			04.9 05.1			59 02	0.0659		255 26	2.0 x 1.5	(99)	355
N lobe S lobe									72 141			145 x 47 100 x 80

TABLE IIIa. — Intrinsic properties.

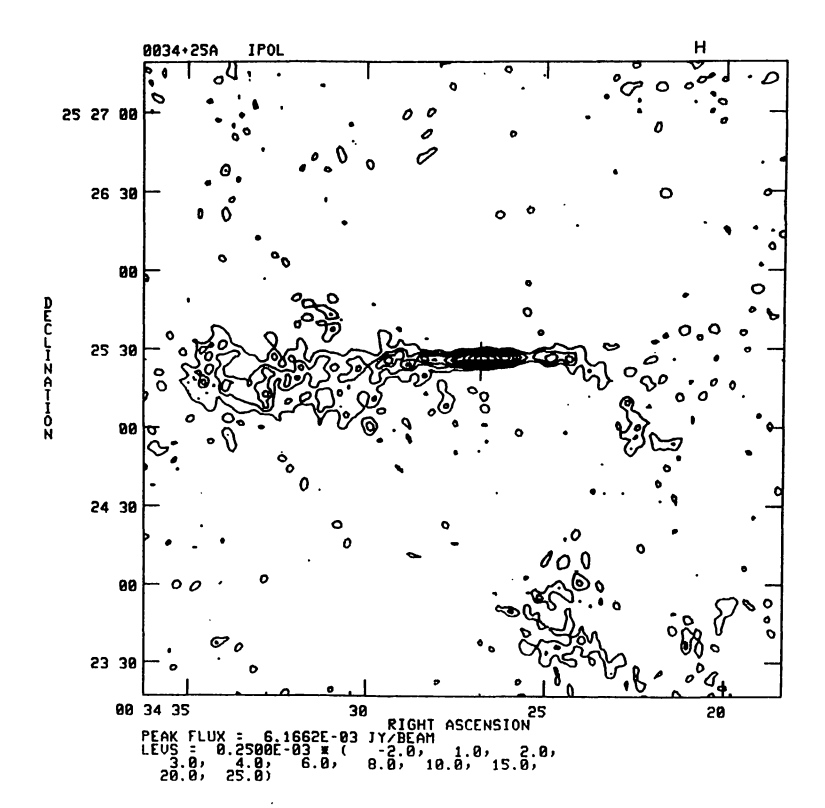
NAME z	M pg	log P 1.4	linear resolution	linear size	u main 3	H eq micro	
			W/Hz	kpc	kpc	E-13 erg/cm	gauss
0034+25 Inn jet E tail WS tail	0.0321	-20.2	23.13	7.4 x 6.1	83 7.2 x 0.8 36 x 20 59 x 11	180 6.0 7.0	14 2.5 2.7
0120+33 NGC 507 E lobe W lobe	0.0164	-20.7	22.30	4.1 x 3.2	31 	4.5 5.5	2.0 2.5
0755+37 NGC2484 core E lobe W lobe E jet	0.0413	-20.7	24.49	6.8 x 6.8	79 .8 x .5 .8 x 27 46 x 27 38 x 34 > 6 x 5.7	20 17	4.5 4.0
0915+32 central N jet S lobes	0.0620	-20.9	24.00*	11.1 x 9.4	275 44 x 36 91 x (12 140 x 29	3.0 12 6.5	2.0 3.5 2.5
1102+30 core E lobe W lobe E jet	0.0720	-20.9	24.27	11.9 x 10.7	160 8 x <.9 66 x 56 66 x 56 >13 x 1.9	6.0 5.5	2.5 2.5
1422+26 E lobe W lobe	0.0370	-19.6	24.00	7.0 x 6.3	72 31 x 31 34 x 34	12.5 11.0	3.5 .3.5

TABLE IIIb. — Intrinsic properties.

NAME	Z	M V	1.4	resolution	1	u min 3	H eq micro
			W/ Hz	Kpc		E -13 erg/cm	gauss
	0.0507			8.6 x 8.0	220 76 x 62 96 x 55 13 x 8	5.5 5.0 24 26	2.5 2.5 5.0
	0.0790			13.5 x 12.0	331 7.4 x 1.3 81 x 61 102 x 20 45 x 7	5.4 19 44	2.5 4.5 7.0
0838+32 N diffuse N compact	0.0680	-22.0	24.47		115 76 x 18 10 x 5 64 x 27	11 216 6.0	3.5 15 2.5
0843+31 N lobe	0.0665	-20.2	23.37	13.6 x 12.6	i 35 x 26 53 x 18	6.0 7.5	2.5 3.0
0922+36 central N lobe S lobe S compact	0.1125	-22.2	24.94	16.2 x 15.7	136 14 x <16 116 x 55 89 x 55 17 x 11	9.0 11.0 42	3.0 3.5 6.5
1005+28 central N lobe S lobe	0.1476	-22.0	24.25		387 44 x 9 92 x 84 109 x 59	3.0 3.5	2.0 2.0
	0.0667	-22.3	24.33	11.4 x 10.2		3.5 4.5	2.0 2.0
1141+37 ME compact MW compact S compact S diffuse	0.115	-21.2	25.30		375 7.2 x 6.5 26 x 18 10 x 4 125 x 97	27 560	21 5.5 25 2.0
central W lobe S lobe	0.0891	-22.1	24.51		315 101 x<11 113 x 45 118 x 85	> 35 4.0 3.5	>6.0 2.0 2.0
1300+32 ME lobe MW lobe S lobe				23.0 x 20.7		25 9 31	5.0 3.0 5.5

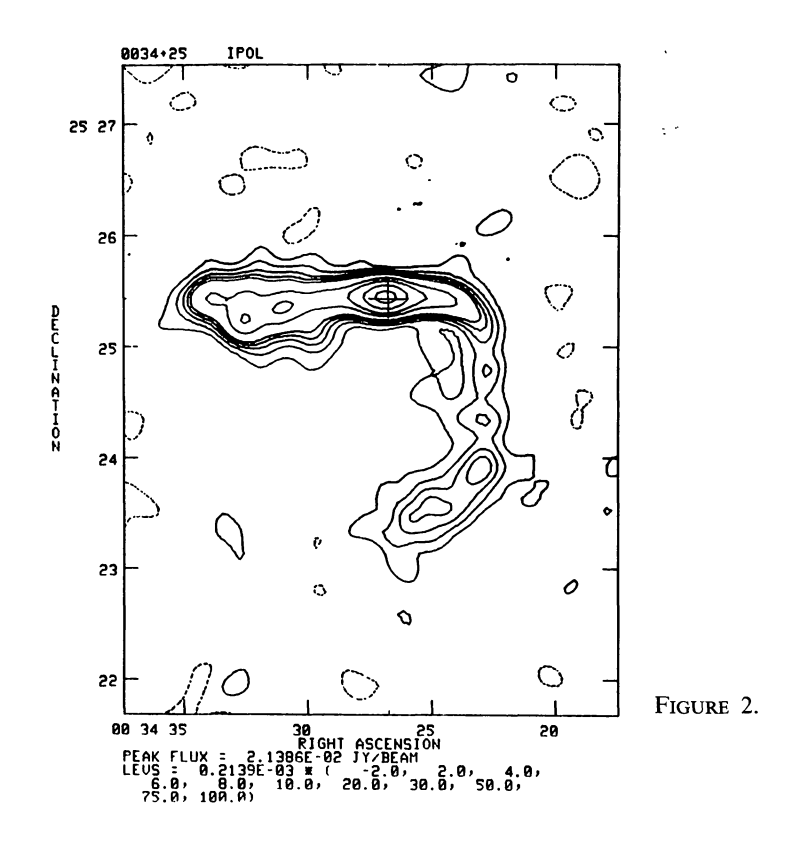
Table IIIb (continued).

NAME	z	M V	log P 1.4 W/ Hz	linear resolution Kpc			H eq micro gauss
1316+29 central E lobe	0.0728	-21.8	24.82	12.2 x 11.3	166 22 x 10 85 x 76	E -13 erg/cm 	3.0
W lobe 1339+26	0.0757	-22.6	24.32	12.9 x 11.9	85 x 62	8.5	3.0
head tail	0.0737	22.0	24.32		69 x 49 137 x 20	8.5 11	3.0 3.5
1357+28 N lobe S lobe	0.0629	-21.9	24.03	11.3 × 10.1	134 45 x 33 50 x 50	8.5 4.5	3.0 2.0
1358+30	0.1104	-22.0	24.63	17.2 x 15.7	238 x 179	2.0	1.5
1441+26 E lobe W lobe	.0621	-22.2	23.97	10.9 x 9.9	173 66 x 41 79 x 50	6.5 3.5	2.5 2.0
1447+27	0.0306	-20.7	22.78		1.6 × 0.6	575	25
1455+28 N lobe S lobe N hot spot S hot spot		-21.6	25.22	22.8 x 20.1	328 162 x 106 162 x 98 17 x 10 25 x 5	4.5 4.5 64 106	2.0 2.0 8.0 11
1512+30	0.0931	-21.9	23.82	15.25 x 13.8			6.0
1521+28 N lobe S lobe	0.0825	-21.7	24.58		232 63 x 63 137 x 53	5.5 7.0	2.5 3.0
1528+29 E lobe W lobe	0.0843	-22.0	24.21	13.9 x 12.8	242 113 x 65 102 x 86	3.0 2.5	2.0
1615+32 3C332 N lobe S lobe Bridge	0.1520	-21.9	25.75	22.2 x 20.1	160 60 x 26 34 x 26 103 x 86	56 44 10	8.0 7.0 3.5
N lobe S lobe	0.1017	-21.8	24.05	16.3 x 14.9	182 73 x 73 88 x 52	3.0 4.0	2.0 2.0
1657+32	0.0631	-21.0	23.65	10.4 x 9.4	59 x 42	6.0	2.
1658+30A core E lobe W lobe W jet	0.0351	-20.6	23.88	10.7 x 9.9	71 1.0 x 0.5 34 x 32 37 x 27 24 x 4	7.5 6.5 80	3.0 2.5 9.3
1658+32	0.102		24.18	15.6 x 15.1	110 x 44	B.O	3.0
	0.1670	-22.4		22.4 x 22.3	212 101 x 92 101 x 92	22	5.0
	0.0659	-21.9	24.07	11.1 x 10.1	101 x 92 309 1.7 x 1.3 126 x 41 87 x 70	3.5 3.5	2.0 2.0



FIGURES 1-11. — Contour maps and radio photographs for sources from the « bright » sample (see text). High resolution maps are distinguished by the letter « H ». The restoring beam is about 13 arcsec for low resolution and 3.5 arcsec for high resolution maps. Levels are in mJy/beam. For two sources (0120+33 and 1657+32) the peak flux given below the contour map is that of another, stronger, source in the field and not of the program source. A black dot in the caption of these contour maps serves as a reminder. The cross marks the position of the optical identification.

FIGURES 12-47. — Same as above, but for the « faint » sample.



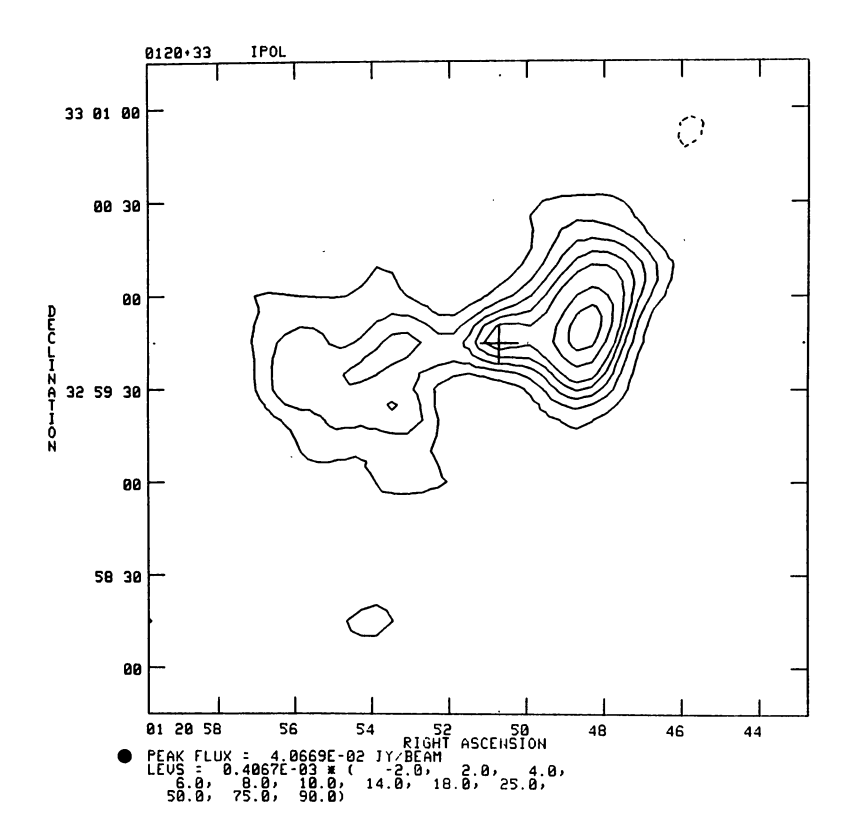


FIGURE 3.

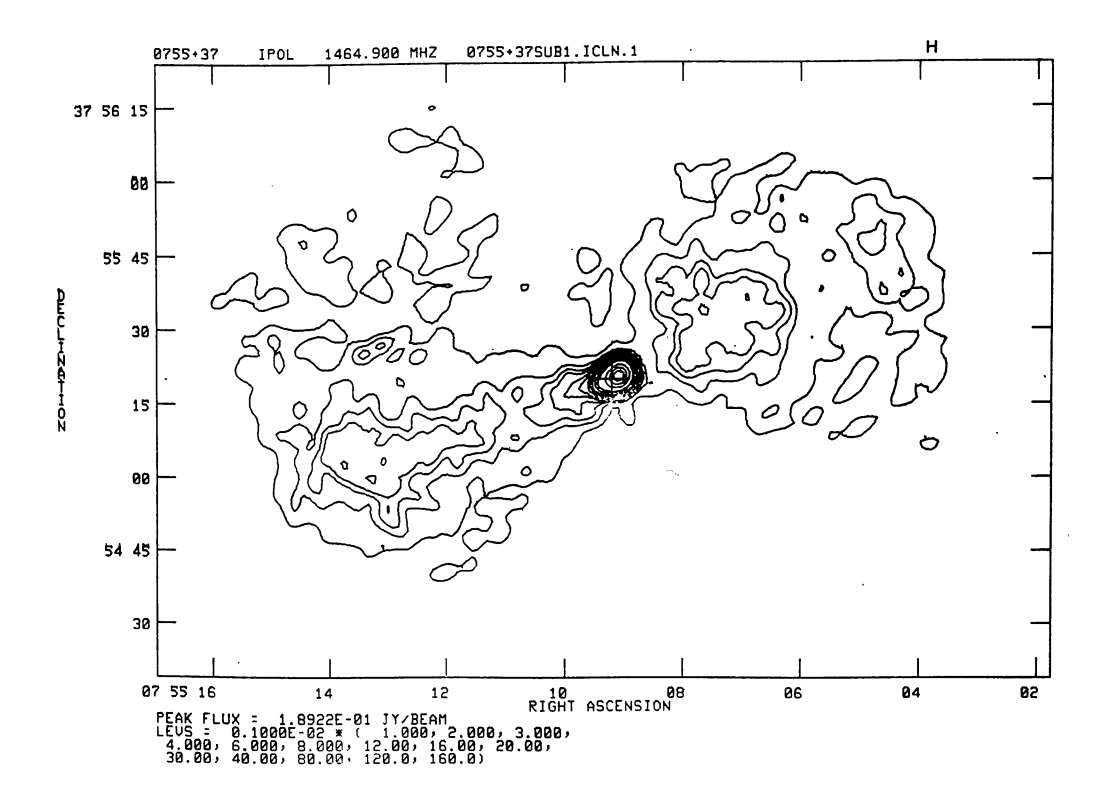
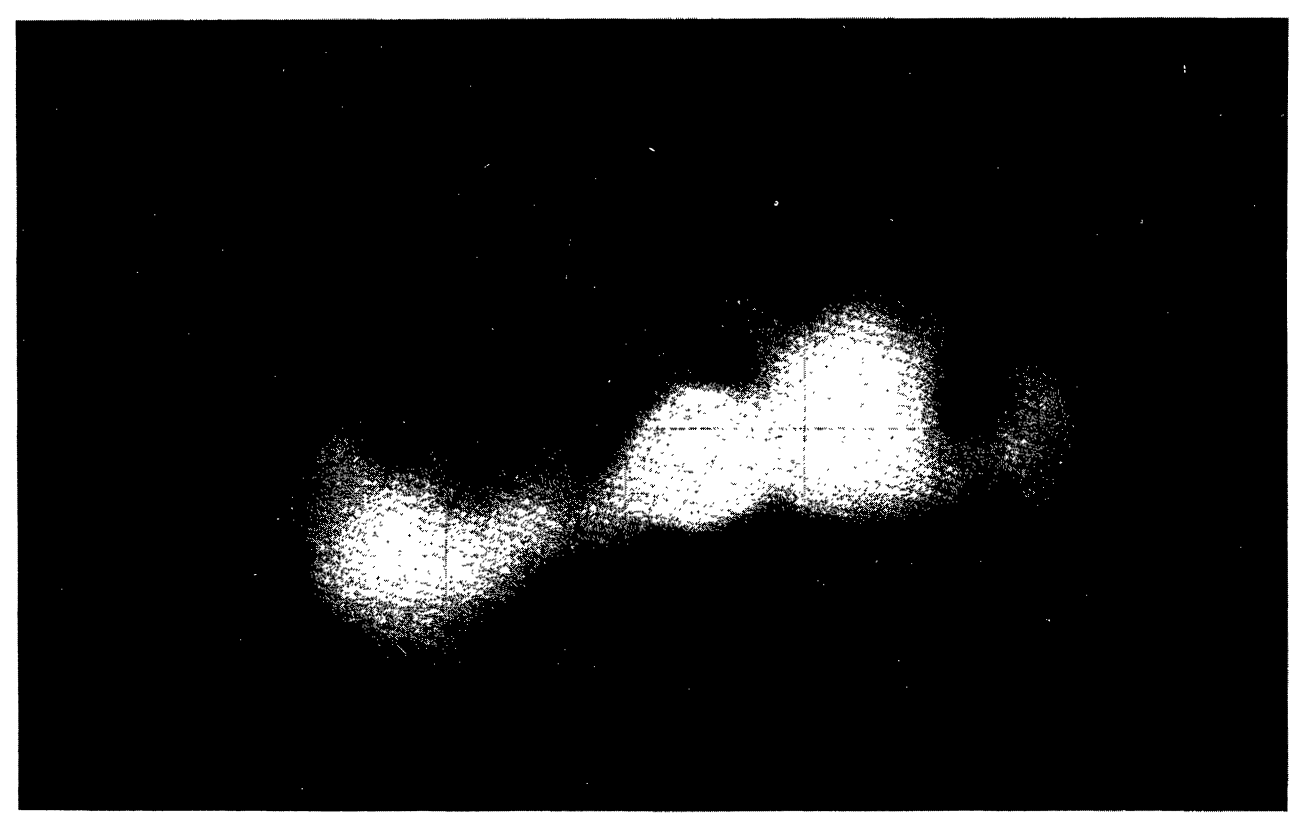


FIGURE 4.



0755 37

FIGURE 5.

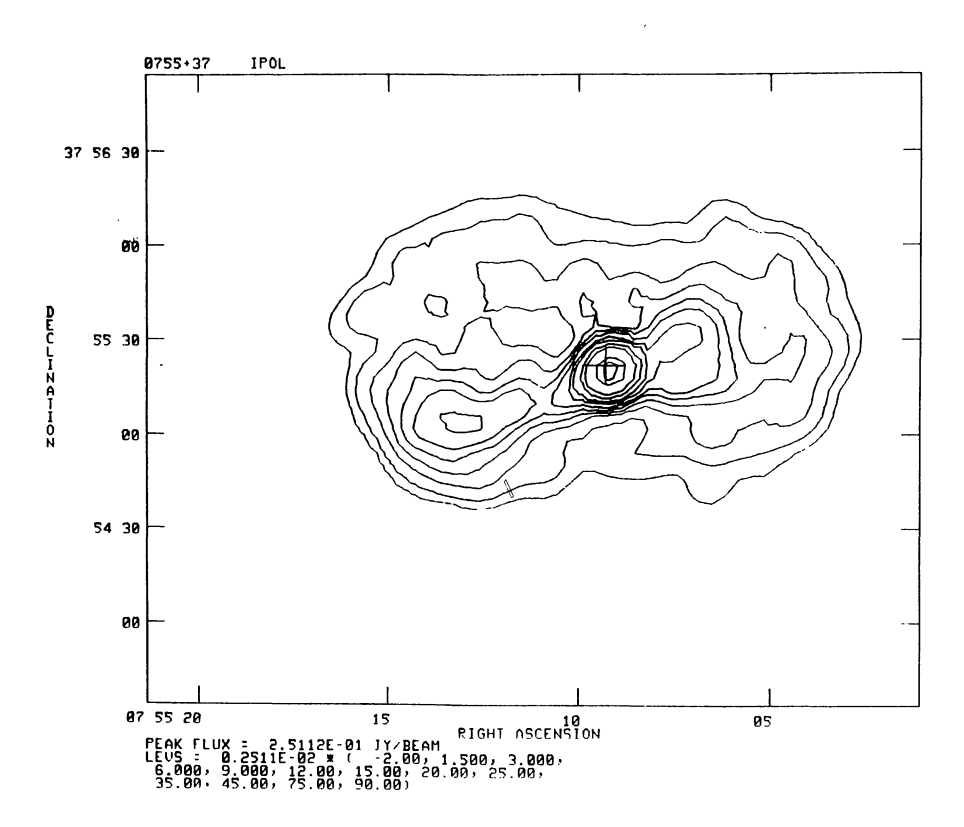


FIGURE 6.

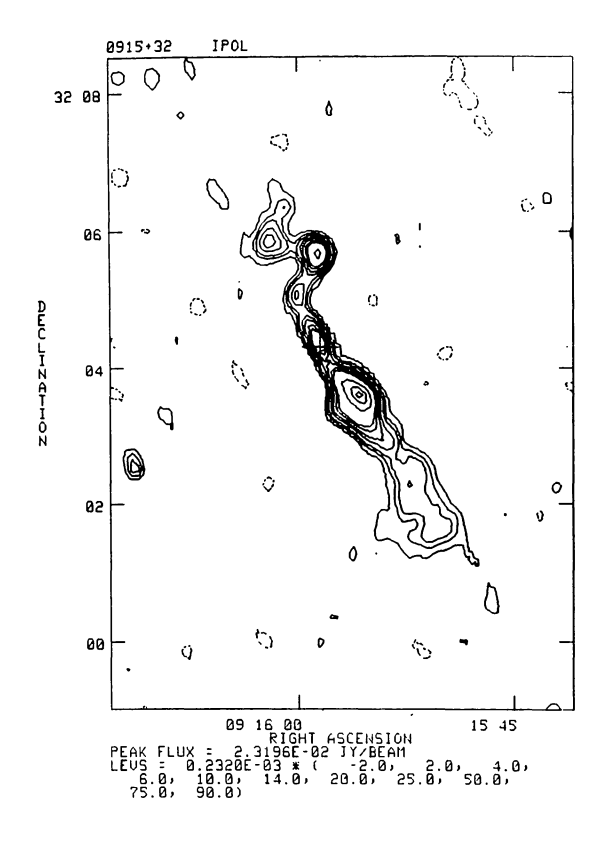


Figure 7.

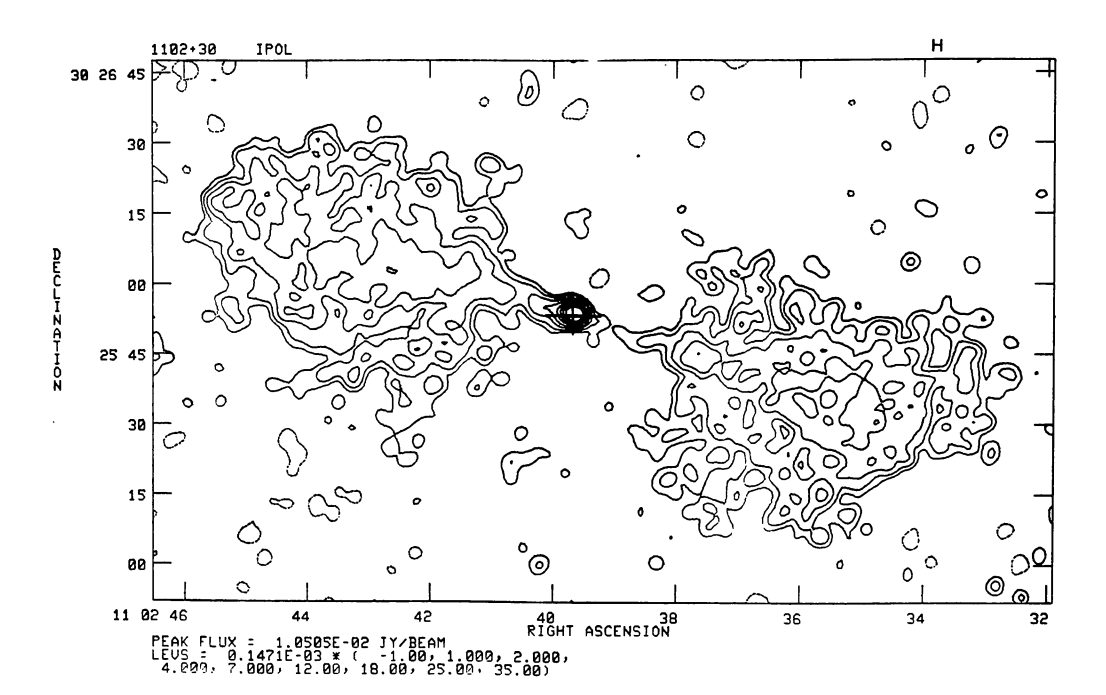


FIGURE 8.

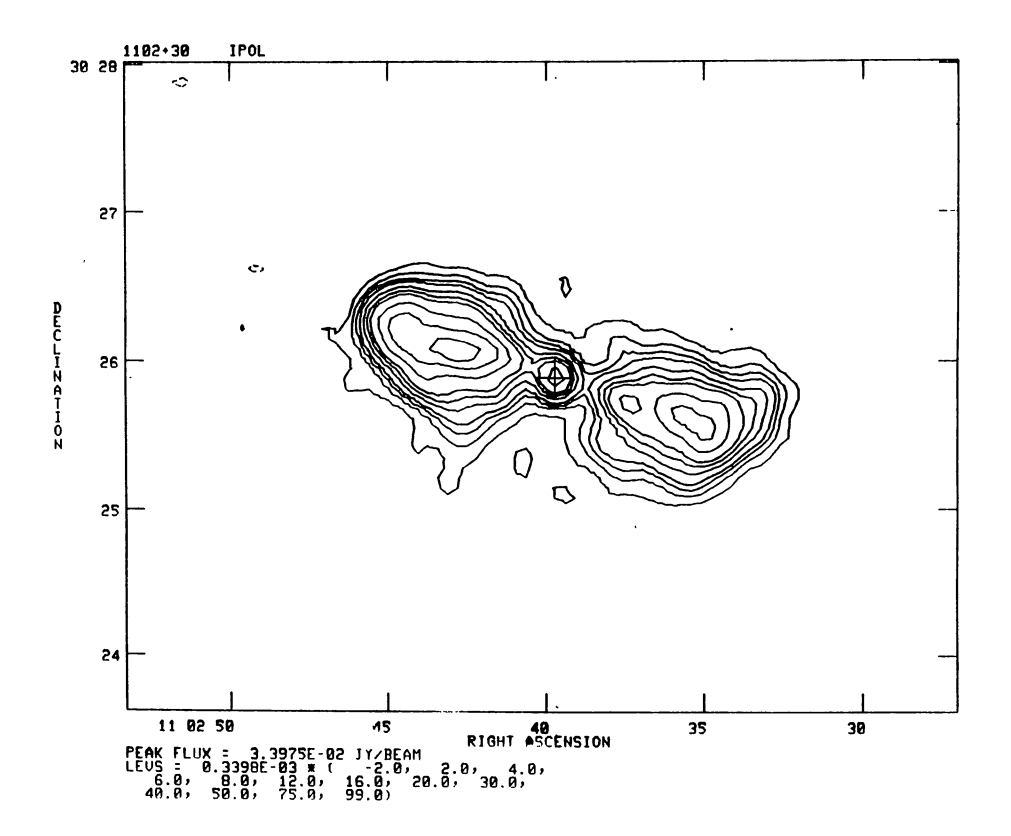


FIGURE 9.

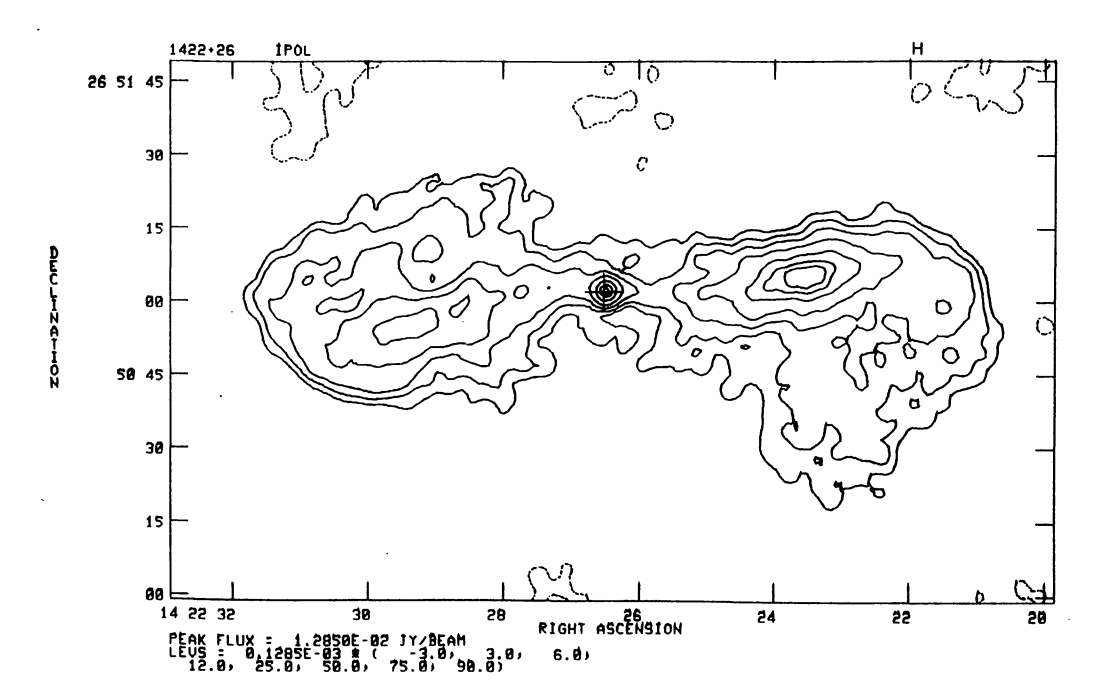


FIGURE 10.

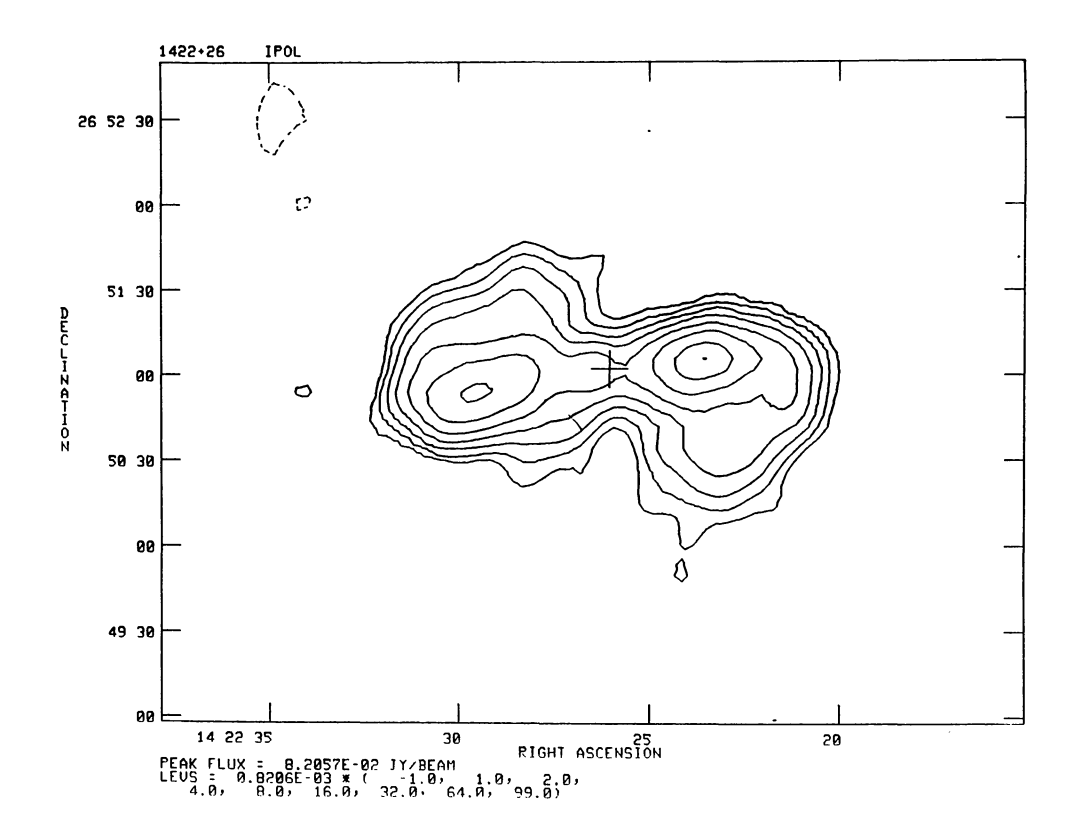
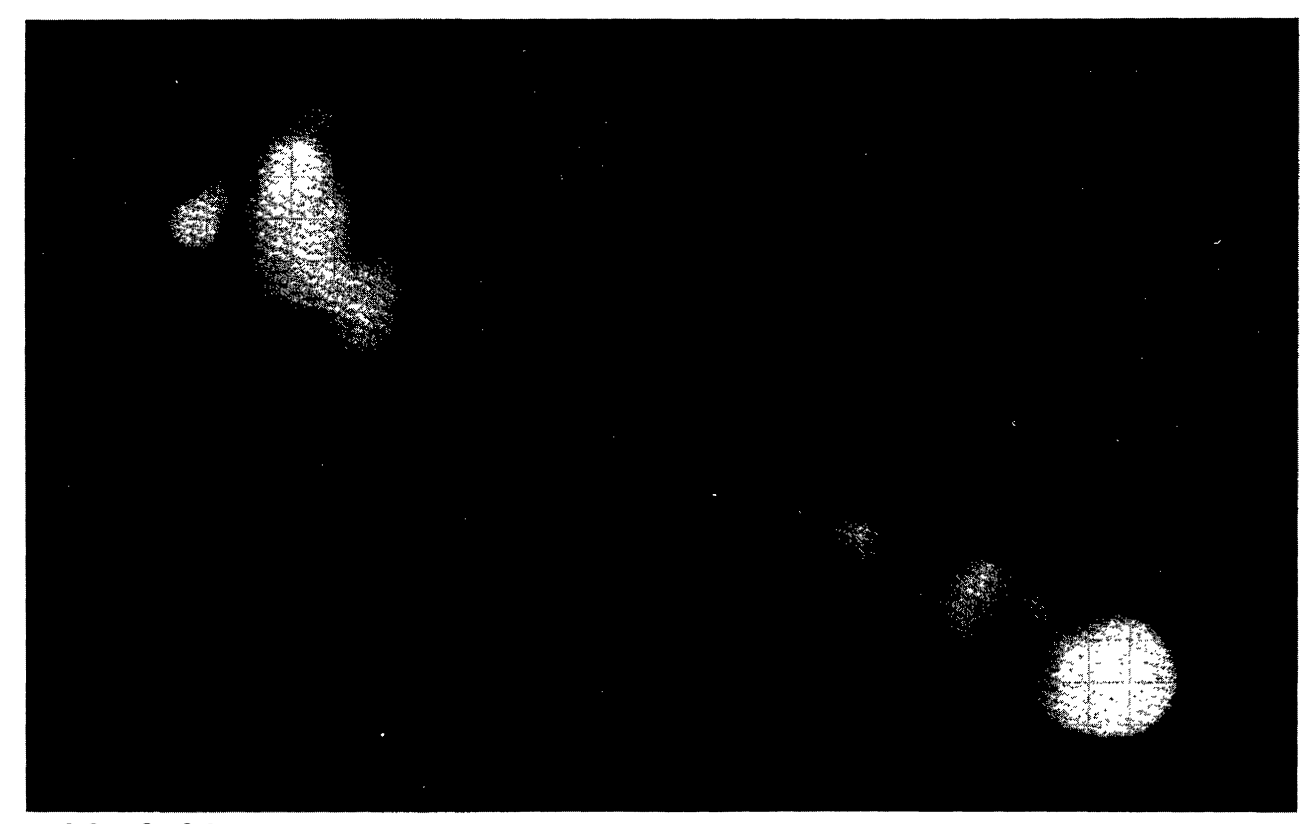


FIGURE 11.



0828 32

FIGURE 12.

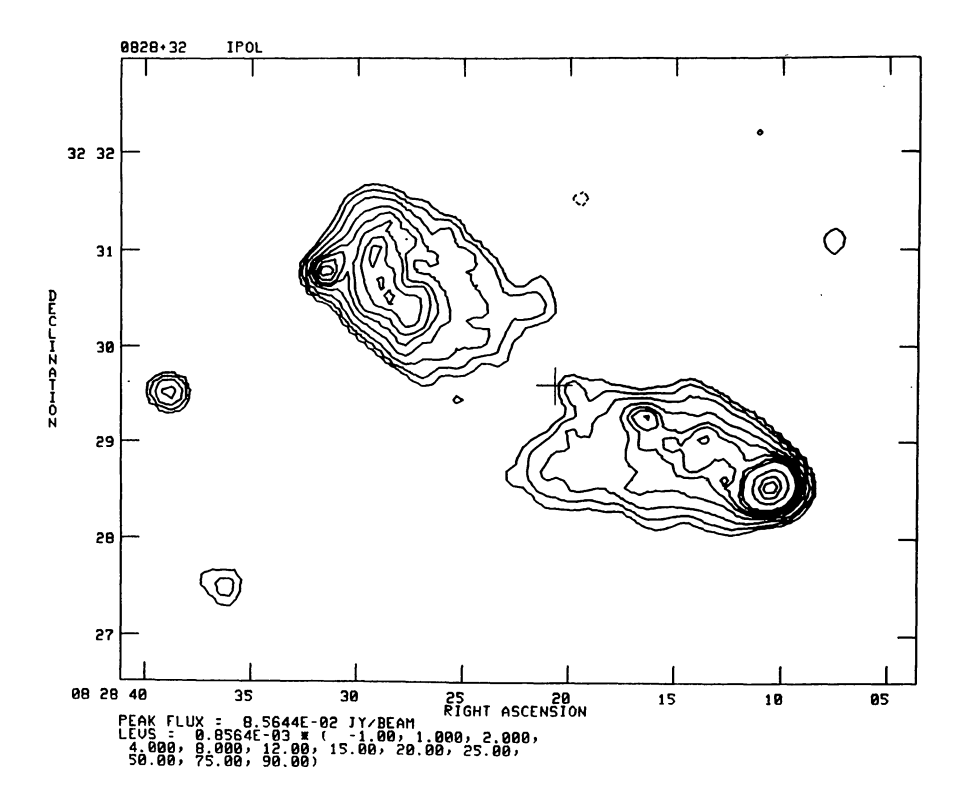


FIGURE 13.

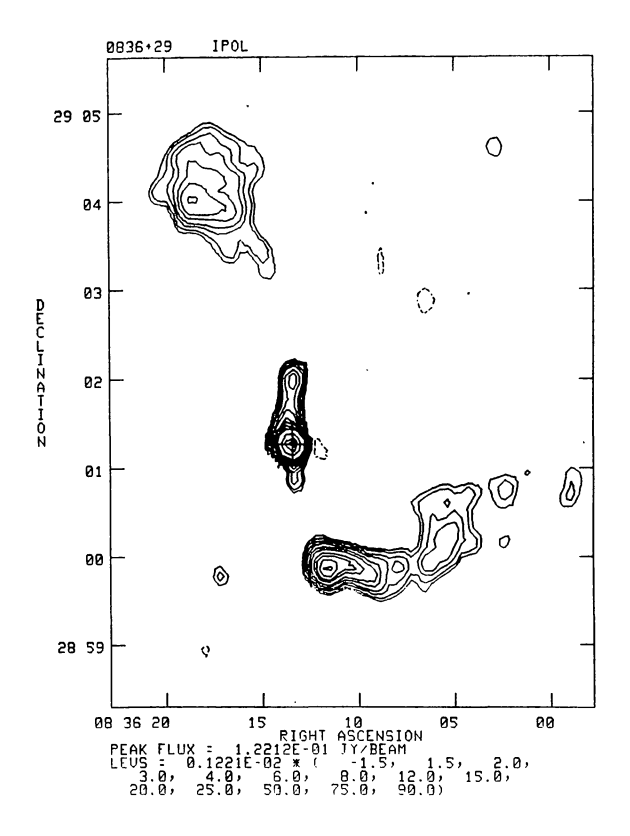


FIGURE 14.

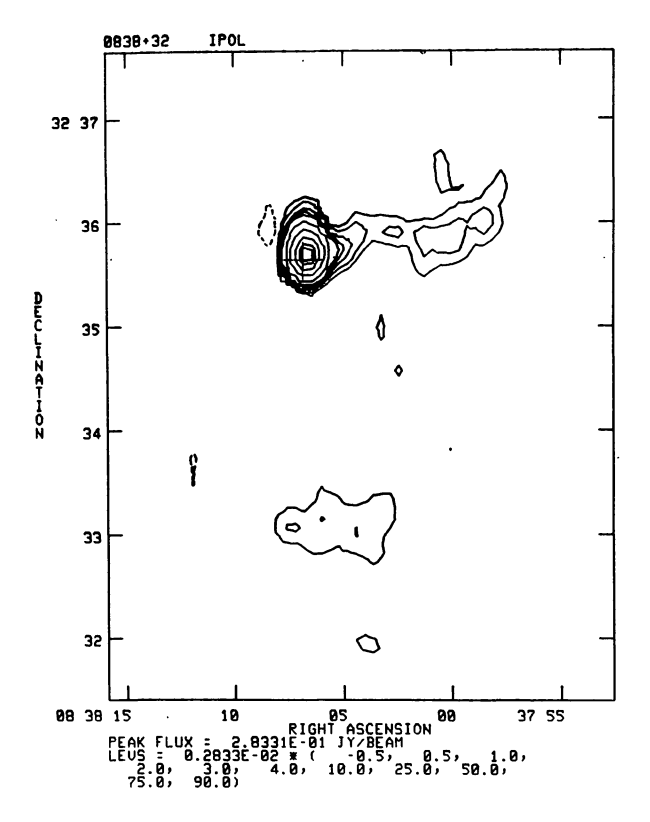


FIGURE 15.

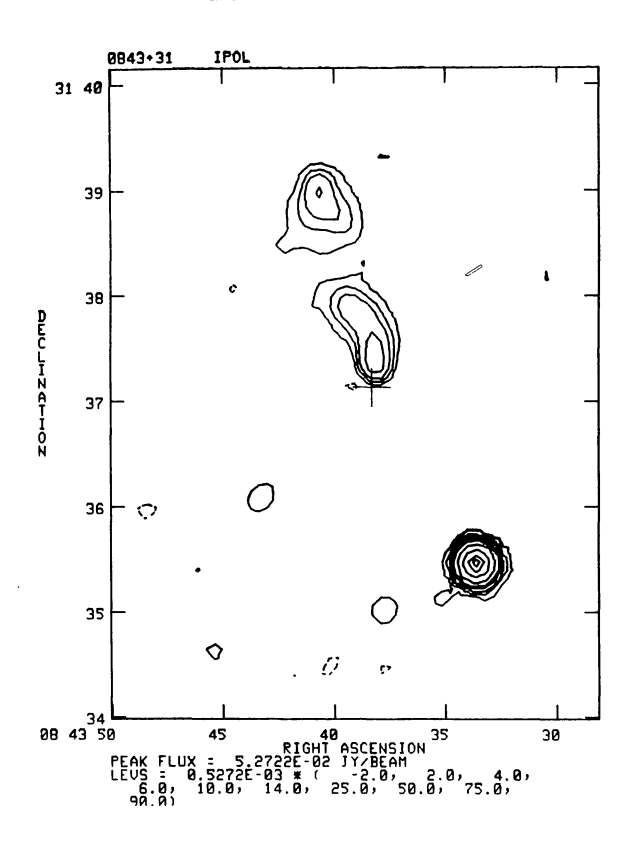


FIGURE 16.

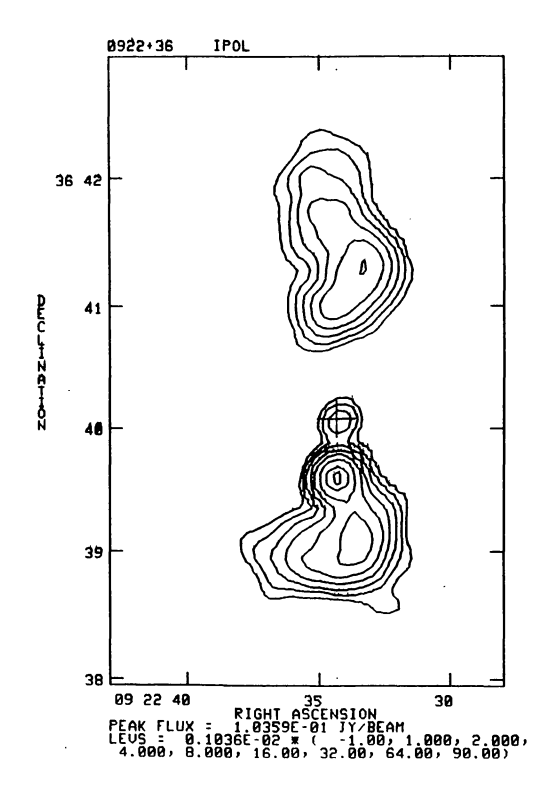
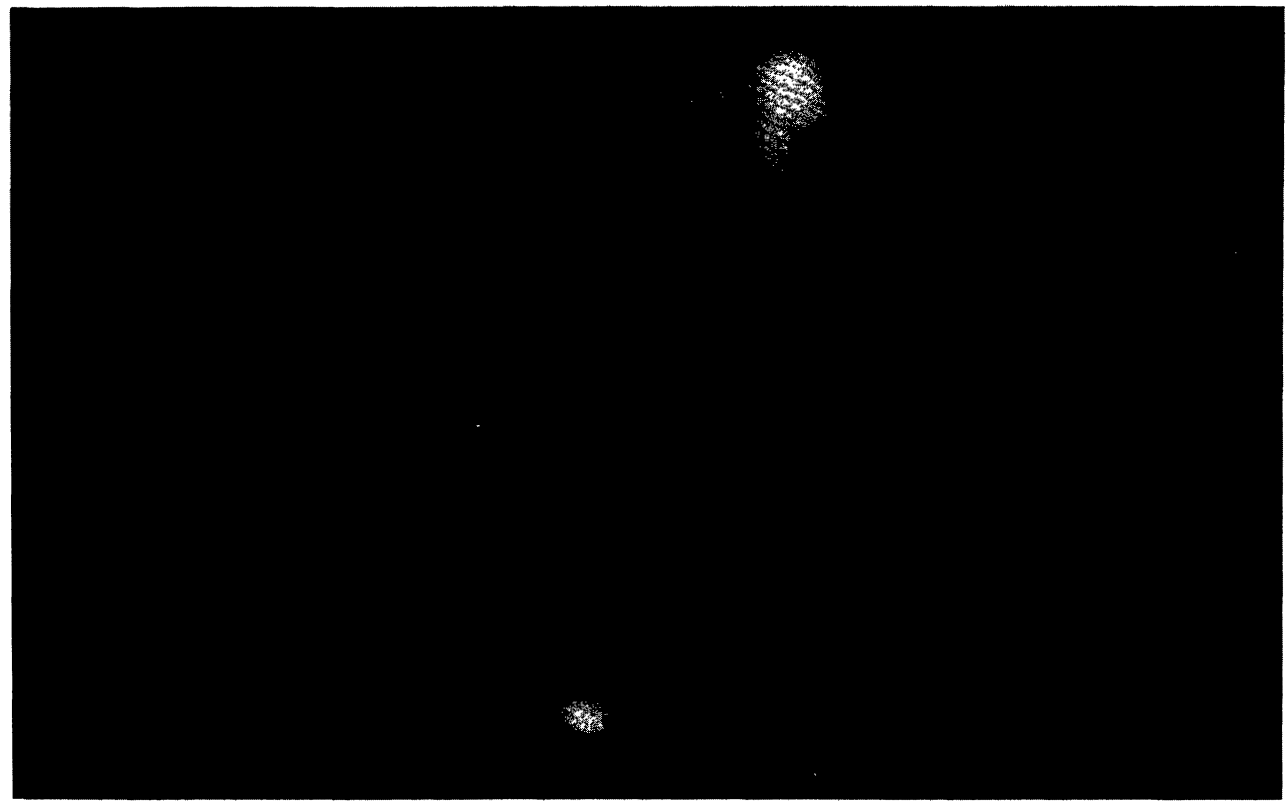


FIGURE 17.



1005 28

FIGURE 18.

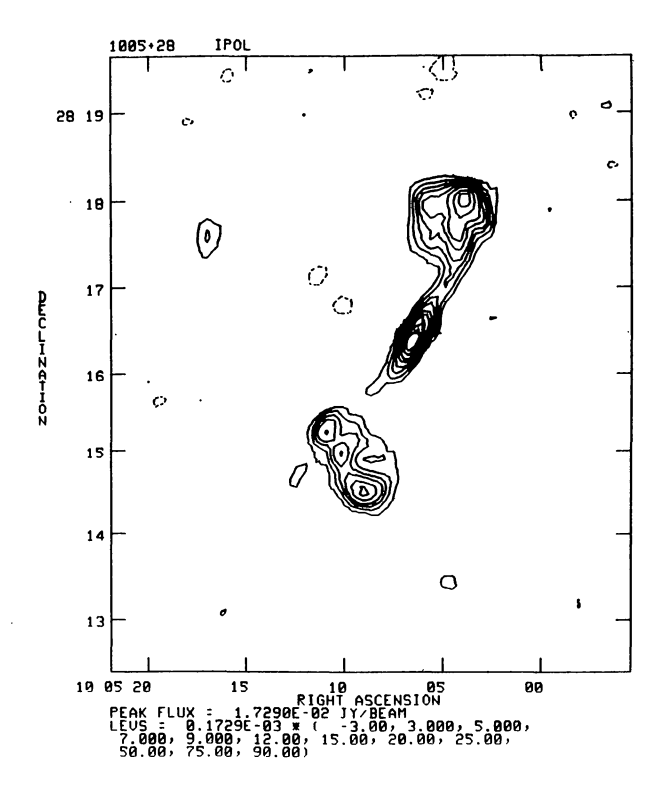


FIGURE 19.



1116 28

FIGURE 20.

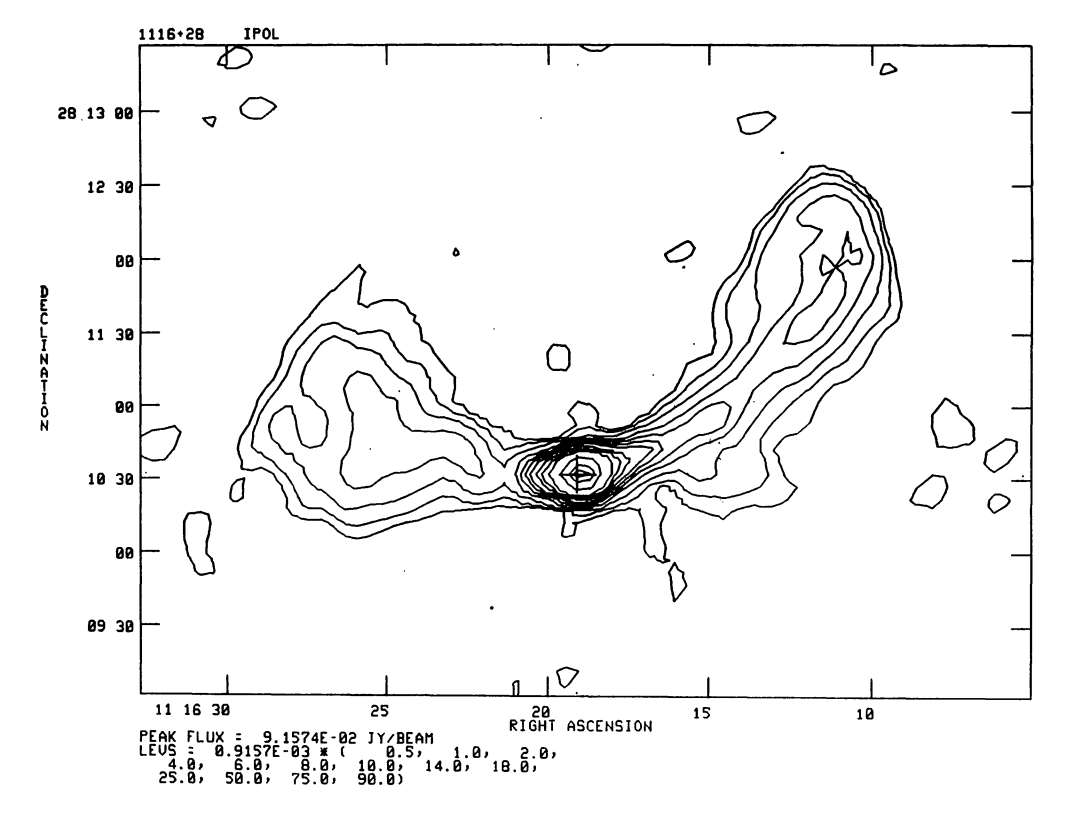


FIGURE 21.

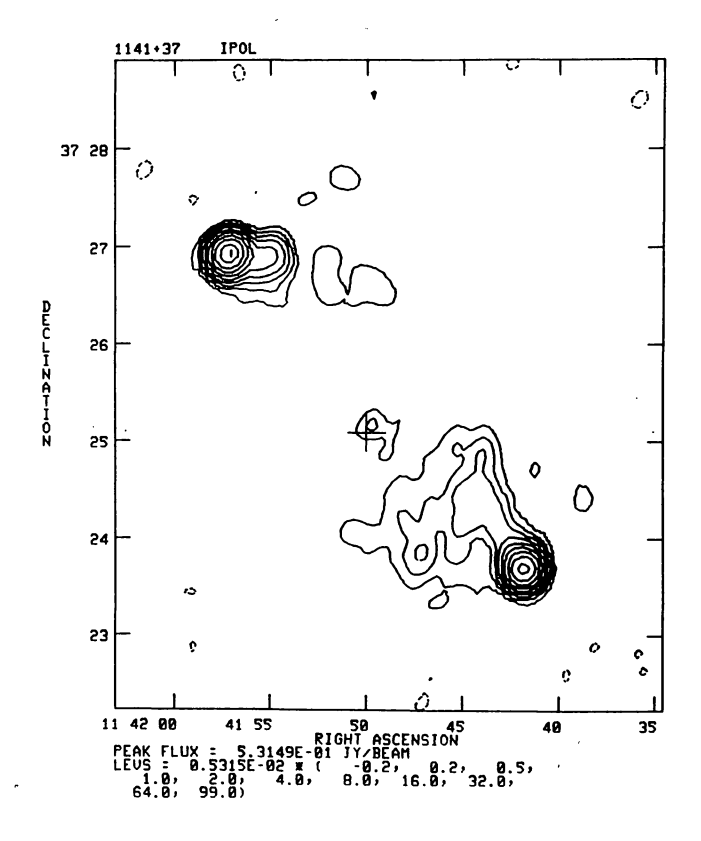


FIGURE 22.



1243 26

FIGURE 23.

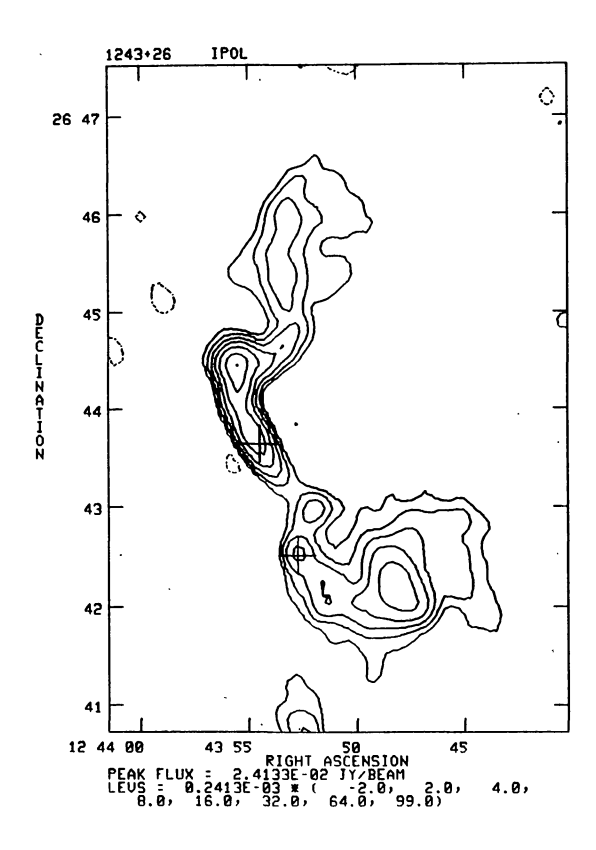


FIGURE 24.



130032

FIGURE 25.

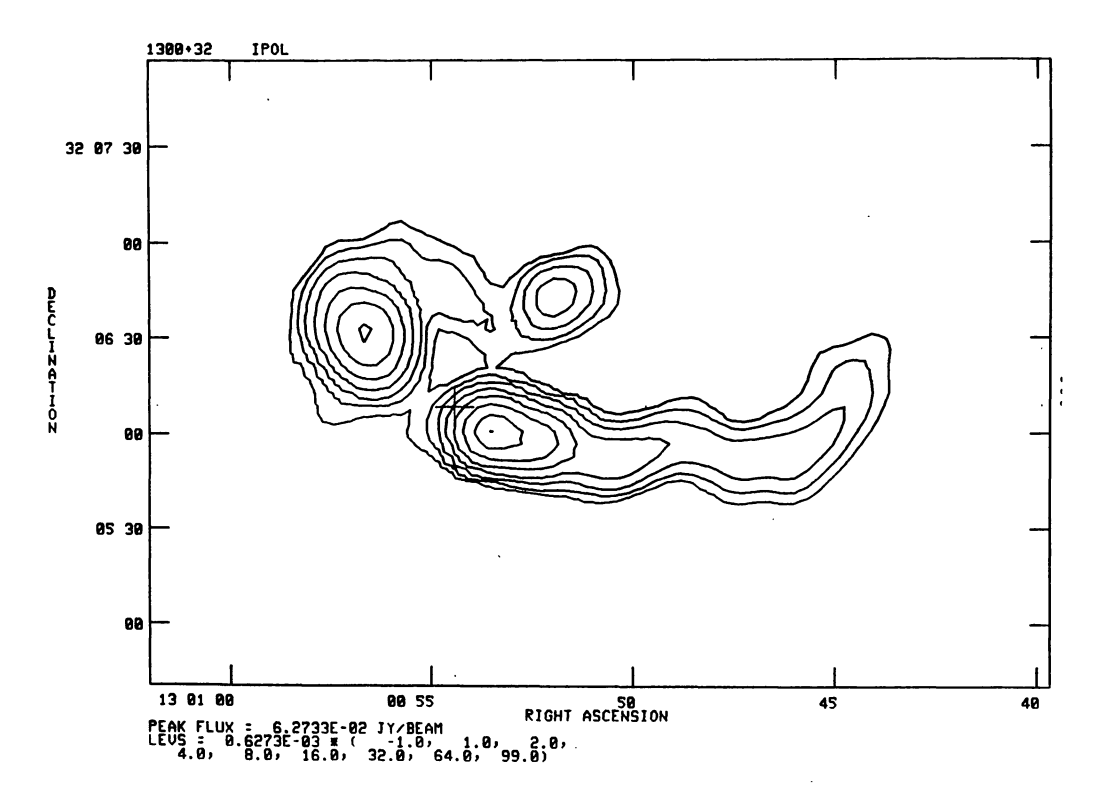
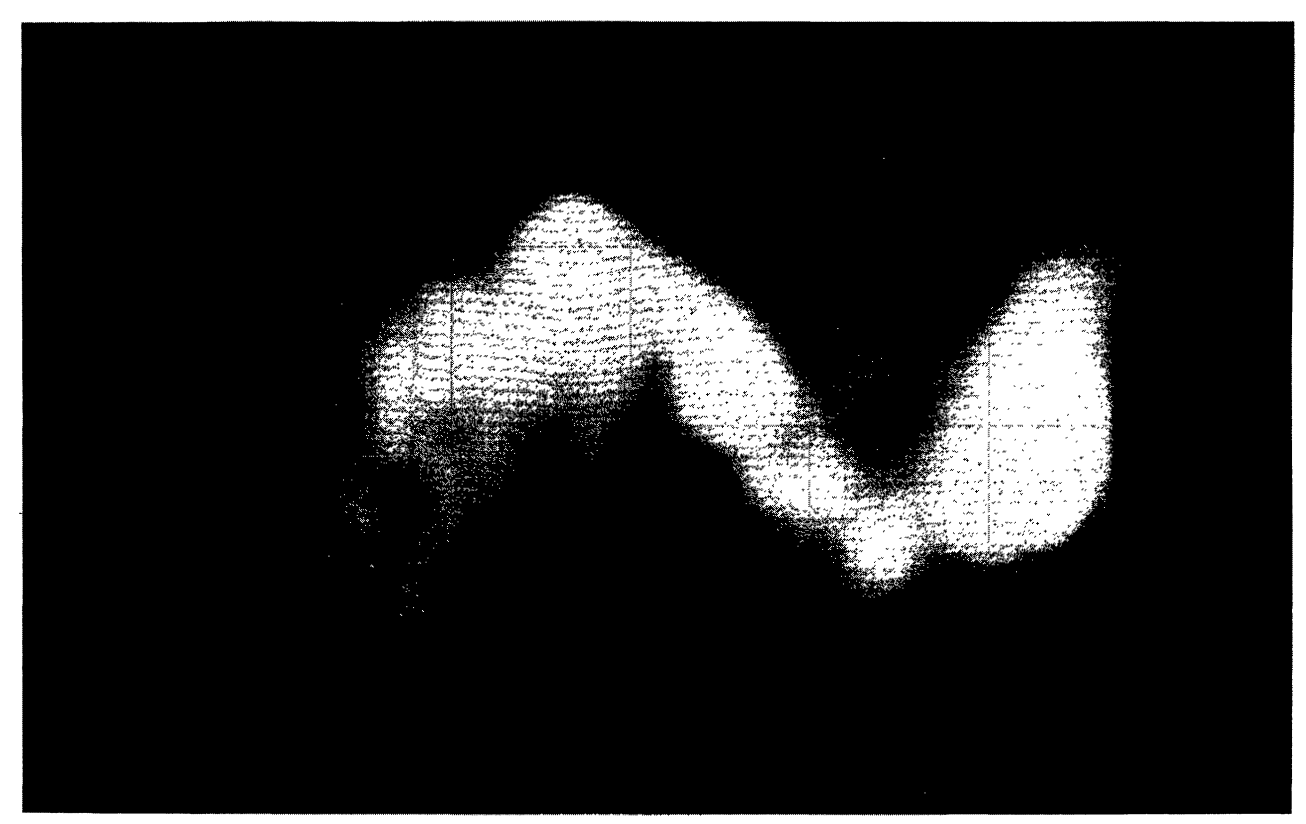


FIGURE 26.



1316 29

FIGURE 27.

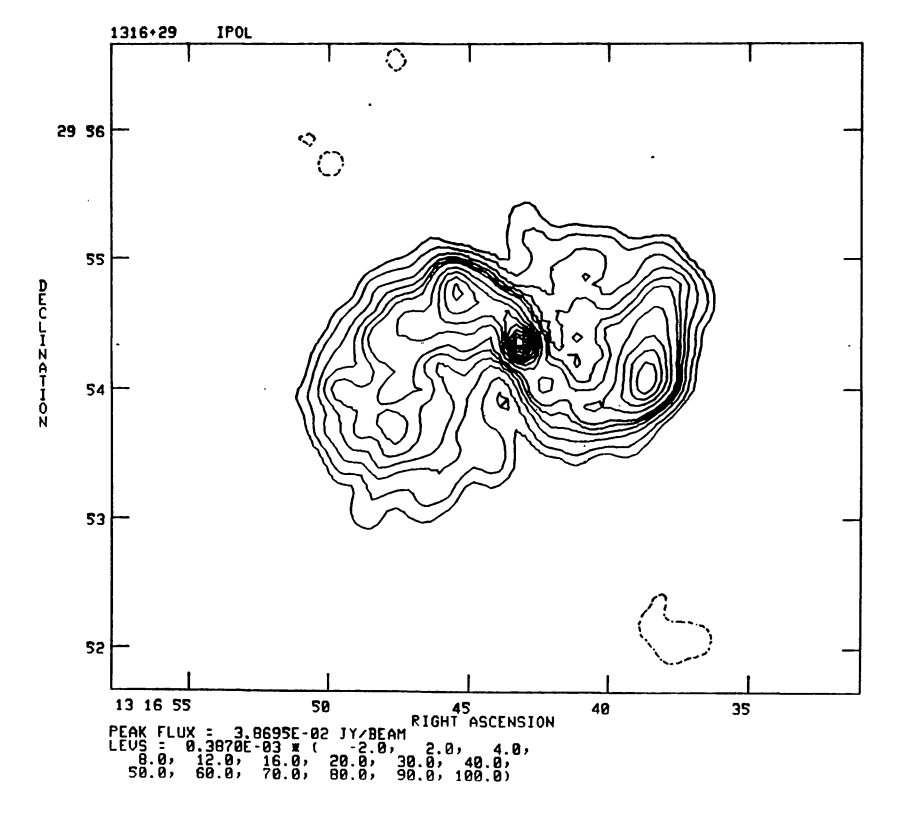


FIGURE 28.

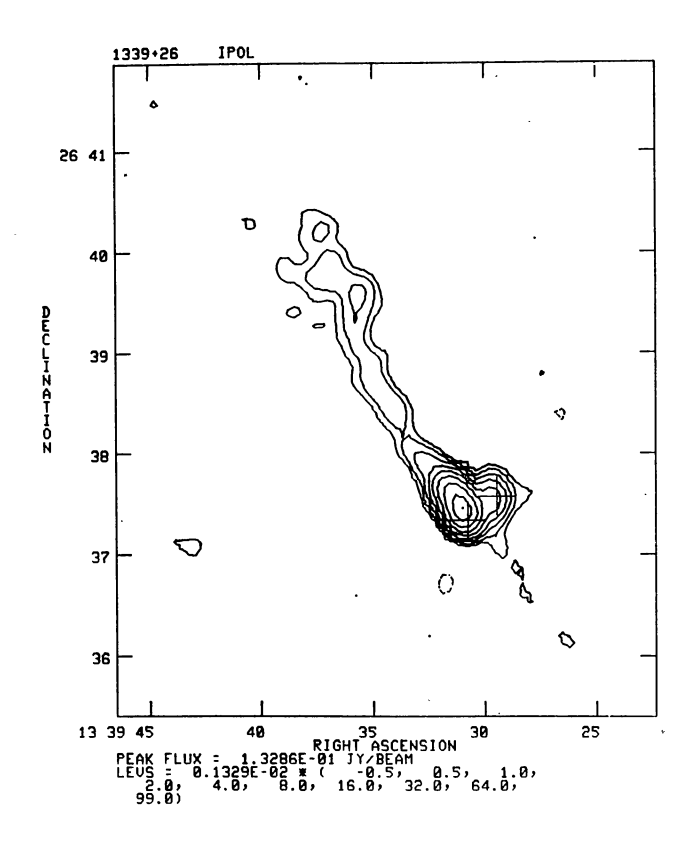


FIGURE 29.

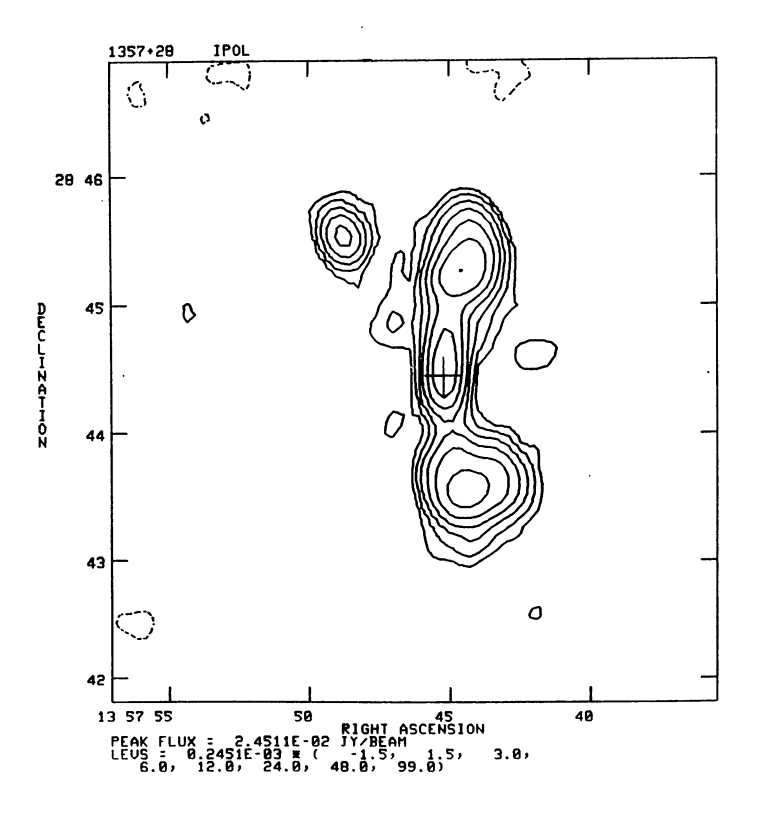


FIGURE 30.



1358 30

FIGURE 31.

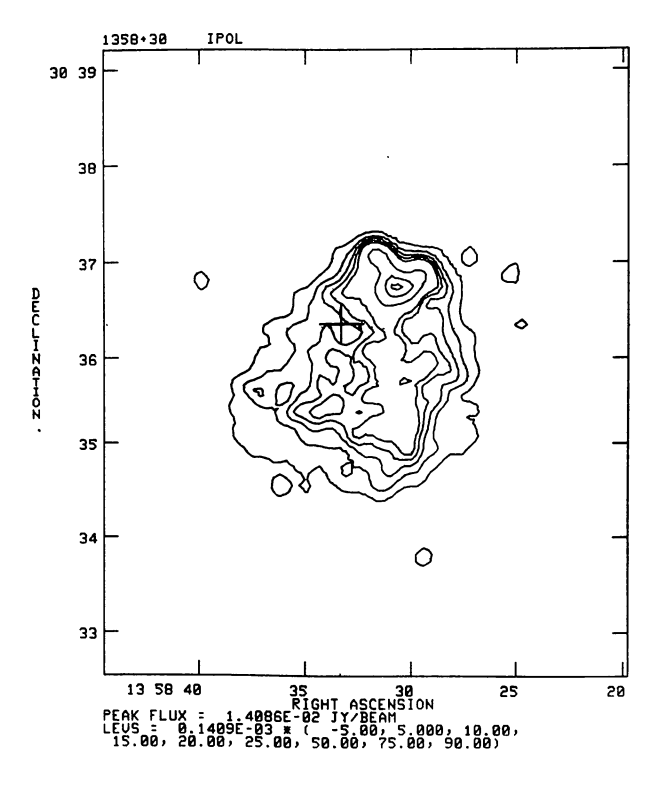


FIGURE 32.

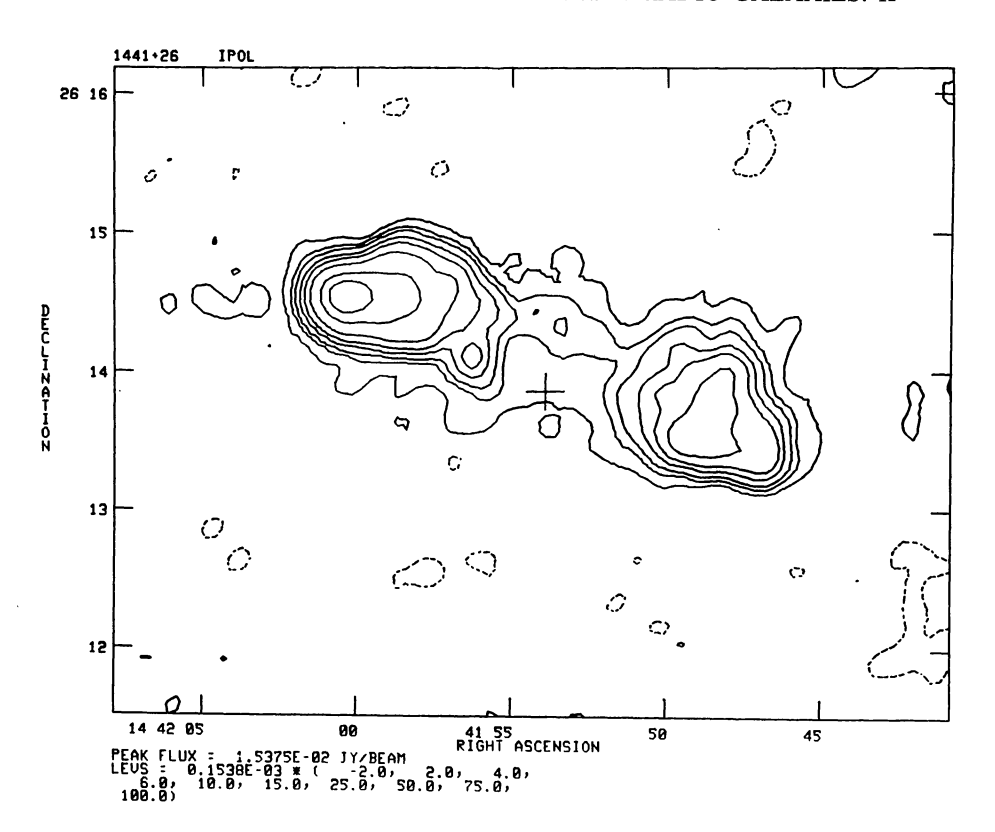


FIGURE 33.

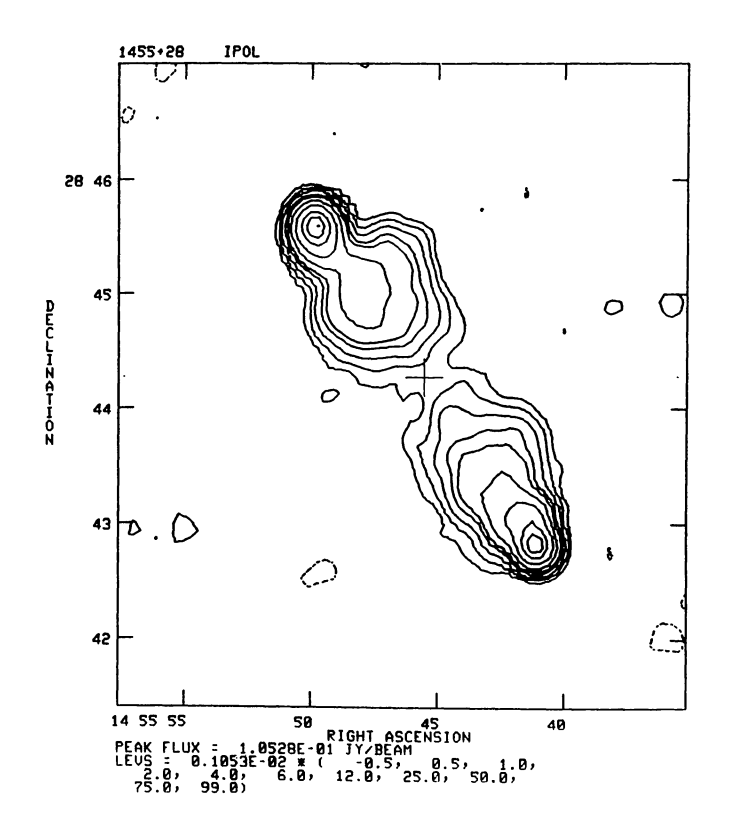


FIGURE 34.

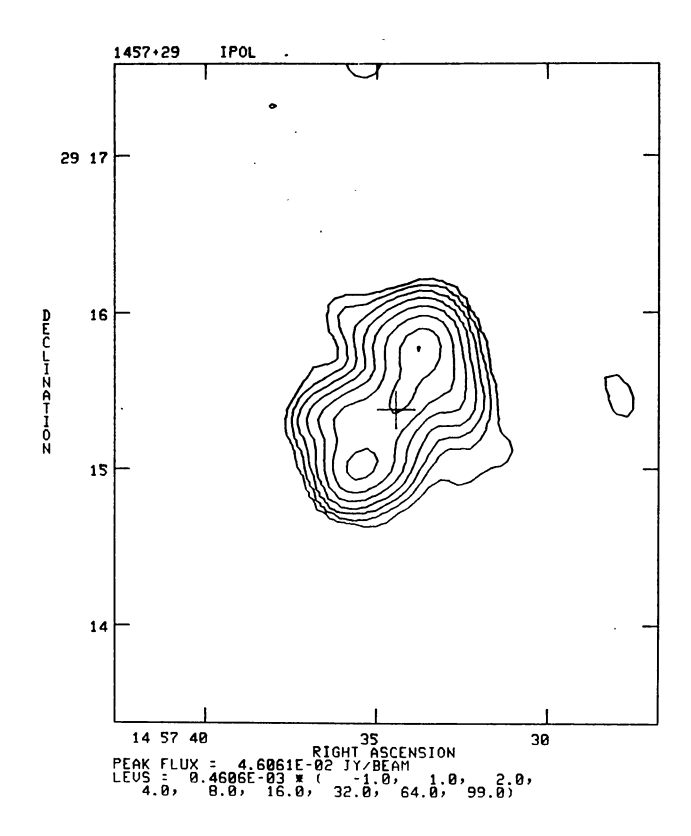


FIGURE 35.

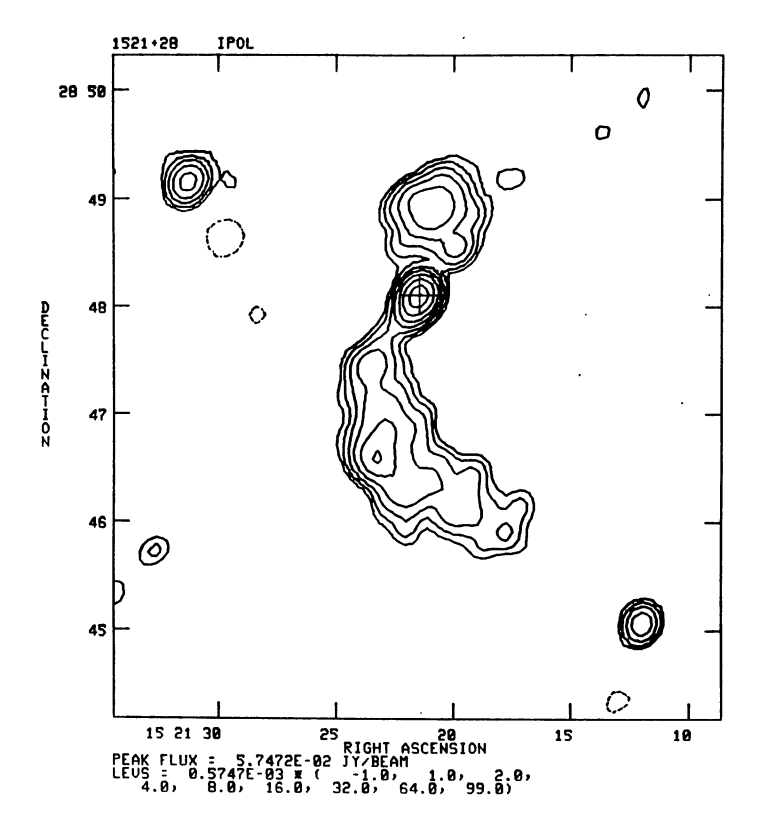
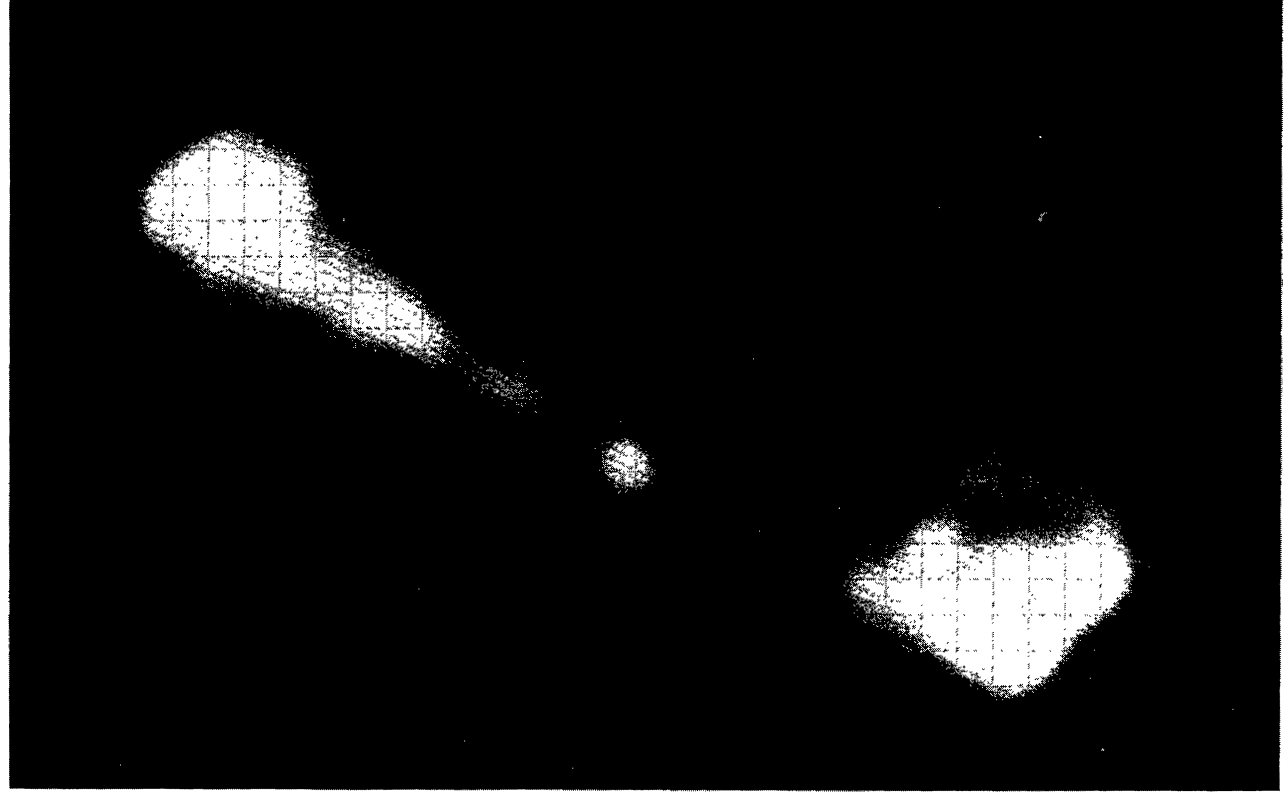


FIGURE 36.



15 28 29

FIGURE 37.

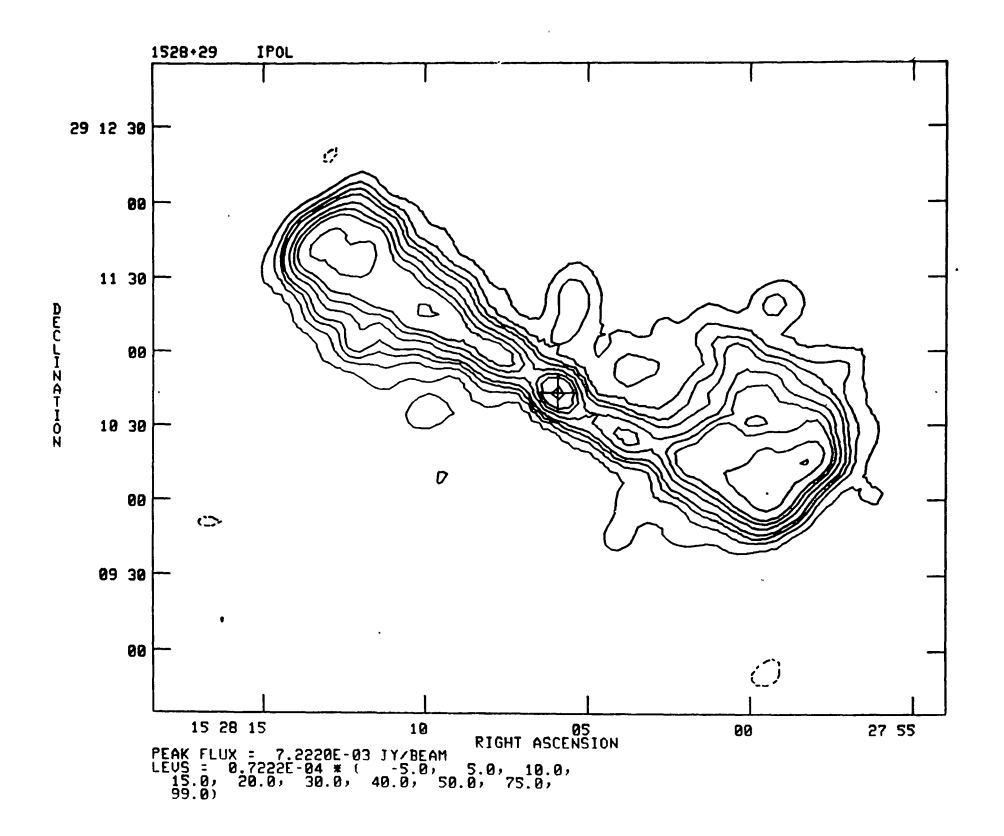


FIGURE 38.

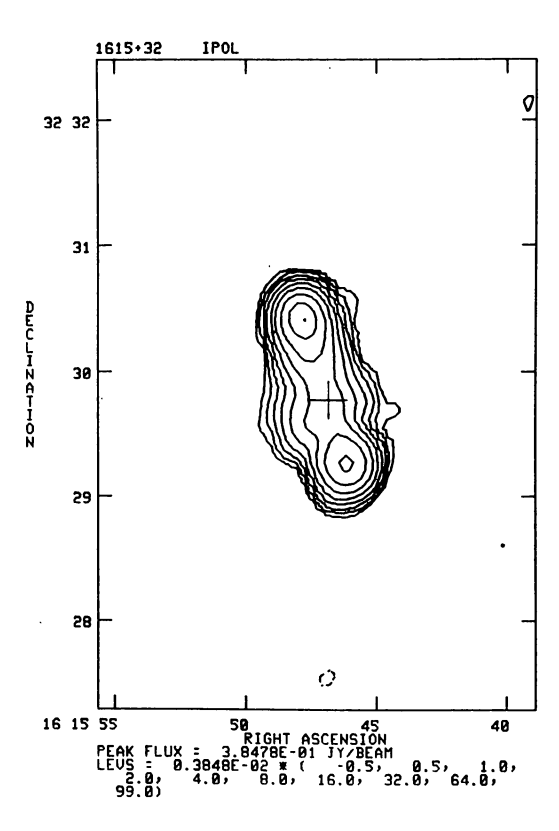


FIGURE 39.

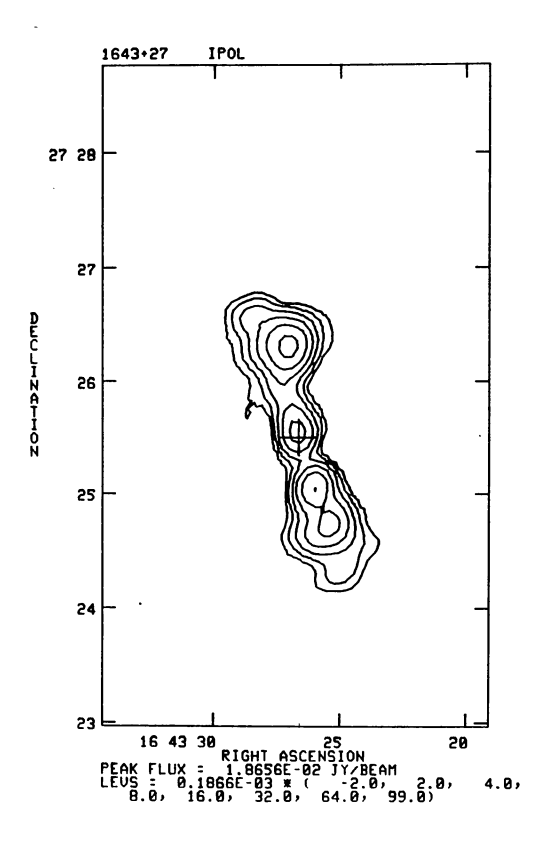


FIGURE 40.

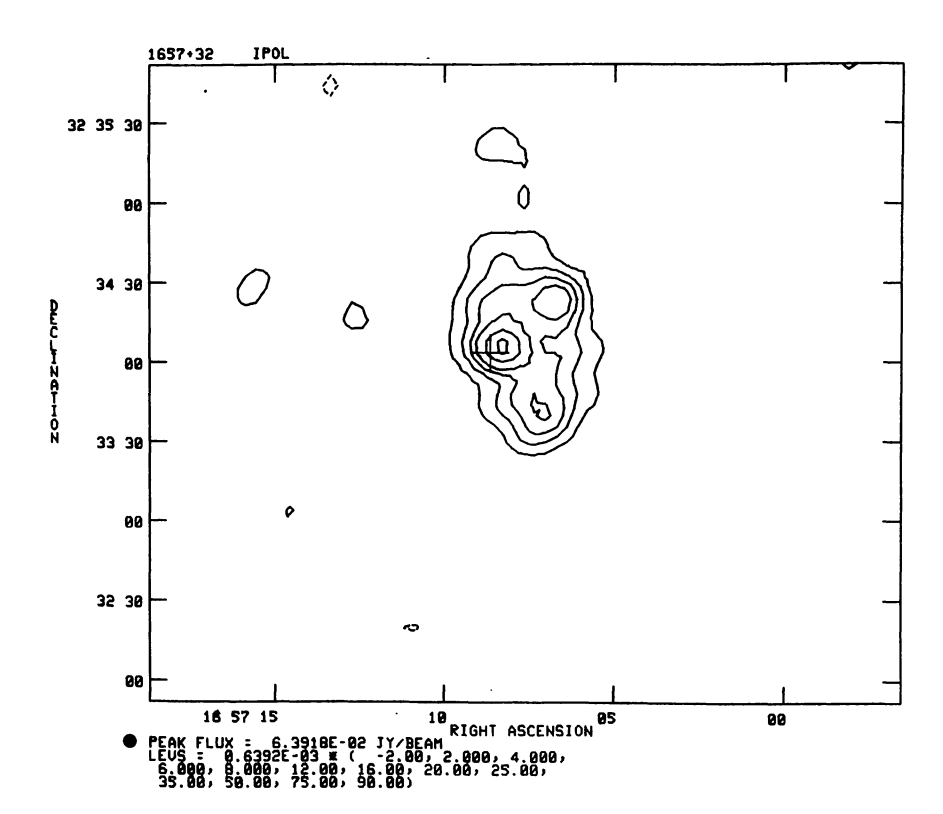


FIGURE 41.

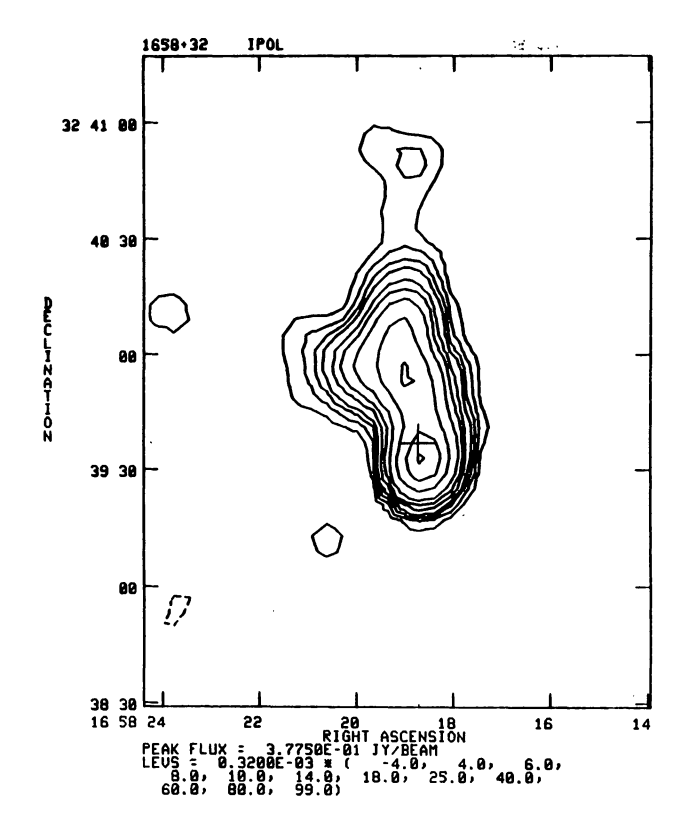


FIGURE 42.



1658 30

FIGURE 43.

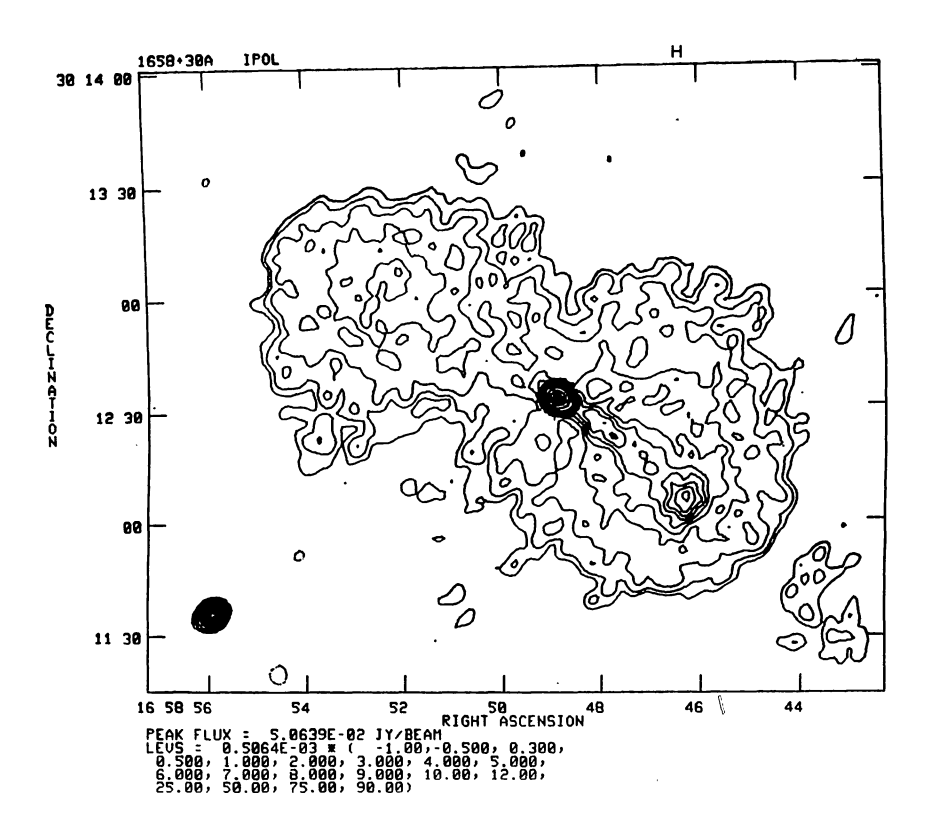


FIGURE 44.

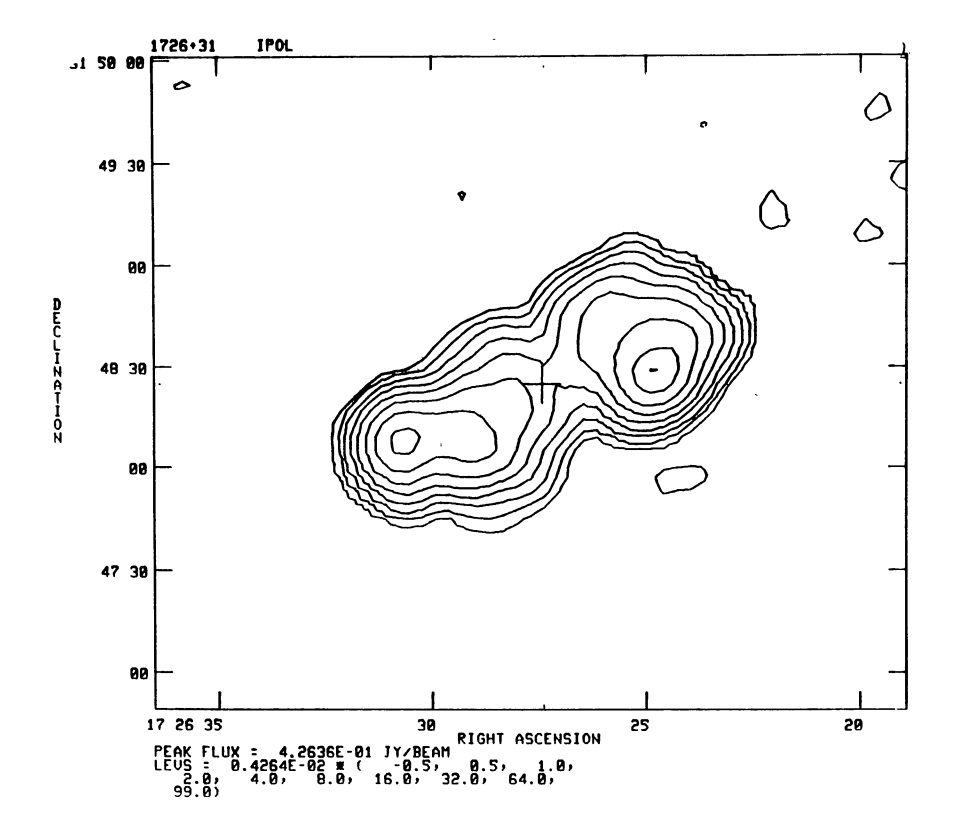


FIGURE 45.

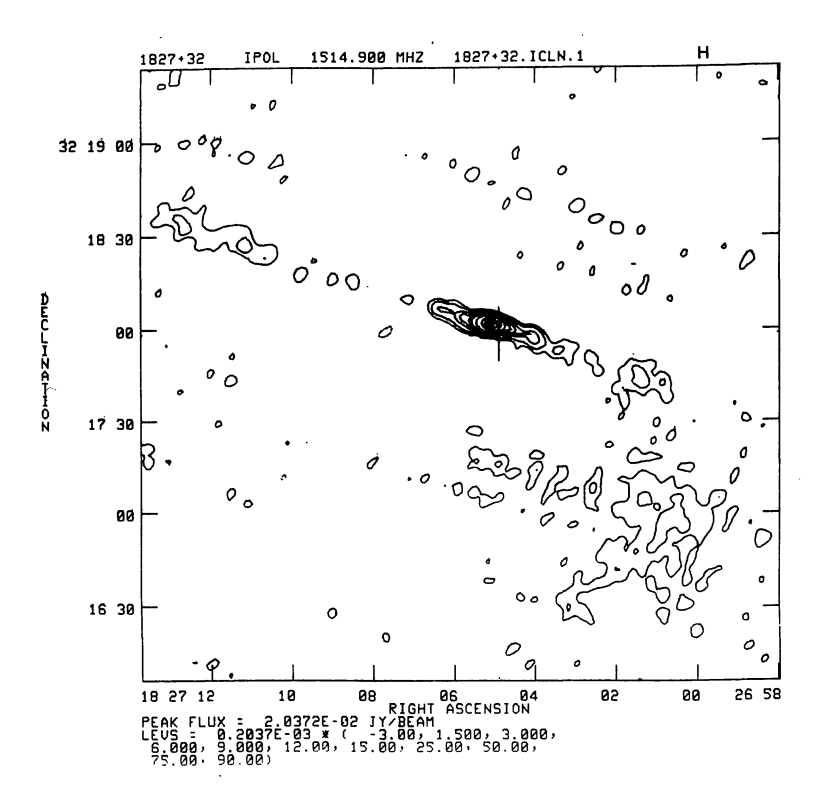


FIGURE 46.

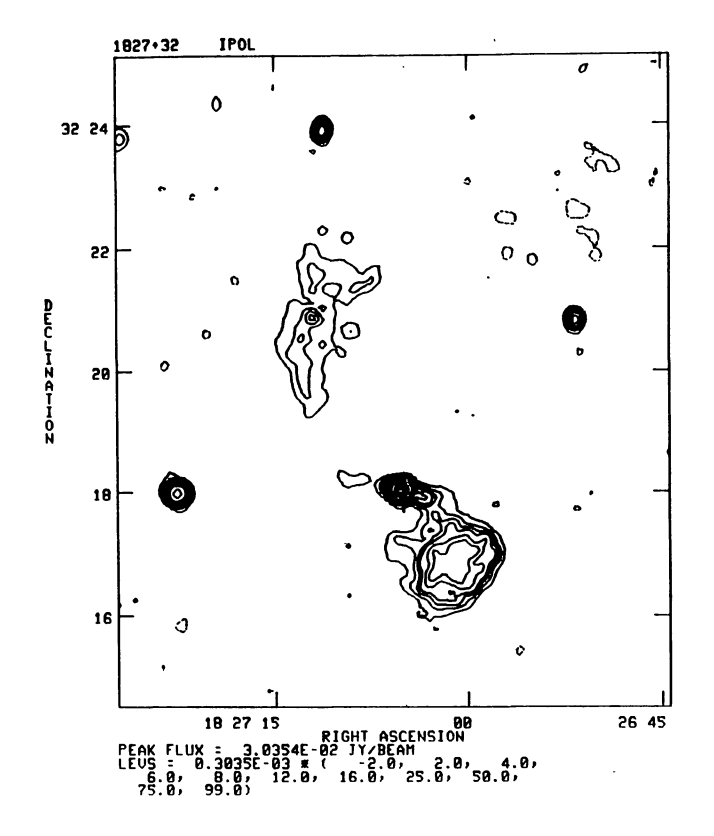


FIGURE 47.